# An investigation in the production of singlet oxygen by titanium dioxide nanoparticles under ionizing photon radiation

by

MM de Jong

to obtain the degree of Master of Science
at the Delft University of Technology.

Student number: 4392825
Project duration: May 1, 2020 – March 29, 2021
Thesis committee: Dr. ir. A. G. Denkova, TU Delft, supervisor
Dr. A. Eelkema, TU Delft
Dr. ir. R. Kruijff, TU Delft

An electronic version of this thesis is available at http://repository.tudelft.nl/.

TU Delft

# Abstract

Most modern cancer treatments are a combination of therapies. In approximately 50% of these combinations radiation therapy plays a prominent role. Although external radiation therapy is very effective, it still damages healthy tissue. Therefore, ways to increase radiation dose deposition at the tumor are sought. The interaction of radiation with the photocatalytic nanoparticle titanium dioxide, $TiO_2$ NPs, is investigated in effort to improve the effectiveness of radiation therapy, minimizing collateral damage to healthy tissue.

$TiO_2$ NPs, upon the absorption of light, are capable of producing reactive oxygen species, which are the main contributor to DNA strand breakage and cell damage through oxidative reactions in radiation therapy. Singlet oxygen is the most potent of these reactive oxygen species. This research aims to determine whether $TiO_2$ NPs are capable of producing singlet oxygen when interacting with ionizing radiation. Efforts are made in uncovering the mechanisms and dependencies behind the production of singlet oxygen using the fluorescent probe Singlet Oxygen Sensor Green, SOSG. The oxidative capabilities of the $TiO_2$ NPs in combination with ionizing radiation are looked into with the probe Mythelene blue, MB, which degrades under oxidative reactions.

The results for aerobic conditions show a significant rise in fluorescent intensity by the probe SOSG when irradiated in the presence $TiO_2$ NPs. The rise in fluorescence appears to be linked to the presence of singlet oxygen but this could not be confirmed. SOSG has also shown a rise in fluorescence in anaerobic circumstances not suitable for singlet oxygen production. This signal response is attributed to the increased presence of hydrated electrons, in line with hypothesized sensitivity of SOSG towards hydrated electrons. The mechanisms behind the production of singlet oxygen could not be uncovered however the production does favour low photon energies and does not depend on dose rate.

The results from the MB degradation experiments indicate no significant amount of degradation is caused by the photocatalytic activity of $TiO_2$ NPs concentrations used in this thesis. The degradation that does occur is due to radiolysis, which favours low photon energies due to the increased absorbance.

The production of singlet oxygen through the oxidation of superoxide radicals, facilitated by the interaction of ionizing photon irradiation with $TiO_2$ NPs, is expected but could not be verified. Future research may verify the origin of the rise in fluorescencent SOSG to be hydrated electrons or singlet oxygen.

# Contents

# 1 Introduction

Most modern cancer treatments are a combination of therapies such as chemotherapy and surgery. Approximately 50% of these combinations contain radiation therapy in a prominent role [1]. Radiation therapy, however, can also result in healthy cells damage. Although advances in radiation techniques have reduced the magnitude of treatment-related morbidity and mortality, novel treatments can further decrease the risk of late toxicity [2]. The objective of this thesis is to study whether it is possible to increase the effectiveness and to improve the selectivity of radiation therapy through the use of nanoparticles.

In this chapter the relevant topics are introduced and the goal of this research is set as well as the research questions. Chapter two, Theory, discusses all relevant topics in further detail as well as the course of action to answer the research questions. In chapter three, Methods & Materials, the experimental requirements are discussed. These include the materials used, procedures followed as well as the available facilities. Chapter four, Results & Discussion, reviews and discusses the results of the experiments set out in chapter two. Chapter five, Conclusion & Recommendations, summarizes these results and where possible states conclusions as well as recommendations for future research on the topic.

## 1.1. Radiation Therapy

Radiation therapy (RT) uses ionizing radiation to deposit energy and kill cancer cells. Ionizing radiation creates electrically charged particles, ions, in cells, which mostly contain water. The ionized water reacts and forms radicals, referred to as Reactive Oxygen Species (ROS), hydrogen peroxide, $H_2O_2$, as well as hydrated electrons, $e^-_{aq}$. These products can interact with DNA strands leading to DNA breakage and cell death [3].

This process is not confined to cancer cells, resulting in healthy cell damage as well. In order to maximize the cancerous cell damage over healthy cell damage, two approaches are important. The first is to maximize the geometrical precision of the radiation, i.e. the area in which the energy is deposited can be optimized by using multiple radiation sources or exploiting the characteristics of different kinds of ionizing radiation [4]. The second is the effectiveness of radiation, optimizing damage towards cancerous cells while decreasing damage towards healthy cells. Healthy cells, for example, are more proficient in repairing radiation caused damages than cancerous cells. This allows for a treatment called fractionation, in which the tumor is irradiated multiple times over a given time. This allows the healthy tissue to heal in between radiation sessions while the cancerous cells accumulate more damage [5].

One possible way to increase the radiation effectiveness is with nanoparticles (NPs). The concept is for the NPs to create more charged particles and ROS in their vicinity, resulting in more cell damage upon irradiation. This can be the result of an increase in radiation absorption by the NPs presence, physical enhancement, or a chemical reaction which results in more cell damage facilitated by the NPs,

chemical enhancement [6]. These enhancements will be discussed in more detail in chapter 1.2 Radiation Enhancement.

Radiation enhancement relies on the fact that the NPs are only present at tumor sites and not in healthy cells when irradiated. This can be achieved by actively placing NPs at the tumor site through intratumoral injection or by the passive aggregation of the NPs at the tumor site after injection in the blood stream [7]. The passive aggregation at tumor sites is possible due to the enhanced permeability and retention (EPR) of nanoparticles in cancer cells. Because NPs enter cancerous cells more easily and leave with more difficulty than healthy cells, a significant difference in NP concentration can be achieved over time [8].

After a significant concentration of NPs is administered to the tumor site, radiation can be applied resulting in the enhancement taking place at the desired locations only. A visual representation is given below in figure 1.1.

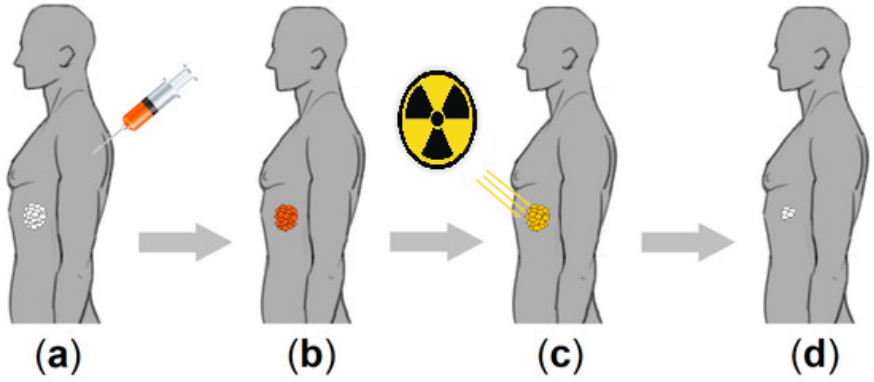


Figure 1.1: The use of NPs in combination with radiation therapy. Step a, the NPs are injected into the bloodstream. Step b, the NPs cluster at tumor sites due to the EPR of cancercells. Step c, irradiation of the tumor with the NPs present. Step D, increased cell damage due to the combination of the NPs and radiation therapy [9].

## 1.2. Radiation Enhancement

Radiation enhancement is the relative increase in radiation effectiveness when NPs are present. The quantity which is increased may vary per object but in this case the goal is cell damage. Cell damage is a result of the reaction of DNA with ROS [10]. The production of ROS is the quantity which should be increased to increase radiation effectiveness. The NP can interact in various ways with the ionizing radiation possibly resulting in radiation enhancement. A visual example is given in figure 1.2 in which hydroxyl radicals, a product of radiolysis is enhanced. The three three general interactions of NPs with ionizing radiation leading to enhancement are discussed in more detail below.

Physical enhancement, depicted by pathway A, is the direct interaction of ionzing radiation with NPs, resulting in an increased energy deposition by the photons. The increase in energy deposition leads to an increase in ROS production as more molecules can be ionized, indicated by the increased amount of free electrons which are the ionizing agents in radiolysis. This is achieved by adding NPs with an increased probability for photon interaction in the medium. Common NPs for this application are heavy as the probability for interaction is mostly dependent on Z, the amount of protons in an atom. This type of radiation enhancement is called physical, as it relies solely on physical processes. The increased radiation effectiveness is linear with the increased absorbance.

No enhancement, depicted by pathway B, or radiolysis is the normal interaction of ionizing radiation with water. The presence of NPs does not influence the quantity of interest.

Chemical enhancement, depicted by pathway C, is an increase in radiation effectiveness as a result of catalytic reactions made possible by NPs. There is a large variety of catalytic reactions which all

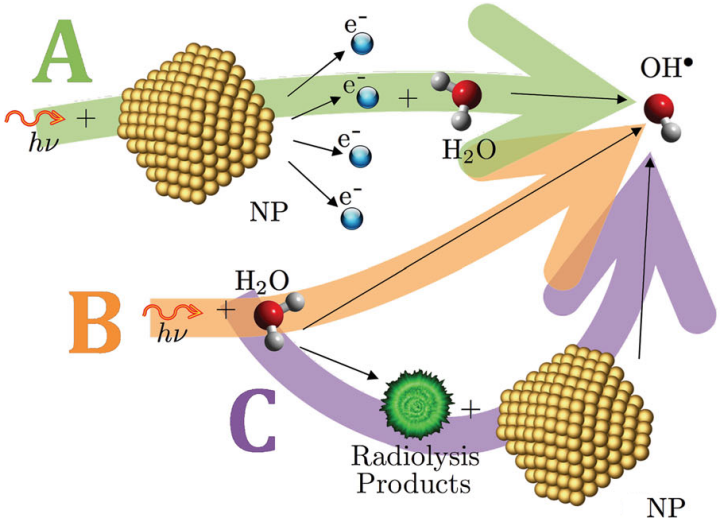


Figure 1.2: A visual representation of the possible interactions of radiation and a NP resulting in the enhancement of hydroxyl radicals, ·OH. Physical enhancement, A, in which the direct absorption of a photon results in the enhancement. No enhancement, B, the NP does not interact with the NP but with water. Chemical enhancement, C, the NP in combination with water or radiolysis products result in the enhancement [11]

result in an increased radiation effectiveness. A commonly made distinction is whether the production of ROS, originally by radiolysis, is catalysed or if the ROS are consumed in the catalytic reaction. If the ROS are consumed in the catalytic reaction a dose rate dependency should be visible as this determines the amount of ROS present at a given moment.

## 1.3. Research Goal

The NP of interest in this thesis is Titanium Dioxide, $TiO_2$. $TiO_2$ is known for its photocatalytic properties, producing electron hole combination upon light absorption capable of creating ROS when interacting with water and oxygen [12]. $TiO_2$ is capable of producing singlet oxygen, $^1O_2$, another ROS which is not created during radiolysis. Singlet oxygen, due to its high reactivity, is understood to play a major role in ROS induced cell damage [13].

Previous research has shown $TiO_2$ NPs to be non-toxic and resulted in an increased dose efficiency when used in combination with RT. The origin for the increased cell damage was assigned to the formation of ROS, but, this was not looked into in depth [14]. Students at the TU Delft attempted to look into the produced ROS. They found an increased amount of singlet oxygen but were unable to draw conclusions due to the possible radiosensitivity of the probes used [15].

This leads to the goal of this research thesis: To determine whether ROS, and specifically singlet oxygen, are formed by photocatalytic $TiO_2$ NPs under ionizing photon radiation. Apart from attempting to prove the presence of singlet oxygen, the possible mechanism behind the radiation enhancement are also investigated.

The presence of singlet oxygen is measured using the probe Singlet Oxygen Sensor Green, SOSG, which is highly specific to singlet oxygen. This probe is claimed to be radiosensitive and therefore many different alterations of the original experiment will be tested in an attempt to circumvent this possible sensitivity.

The probe Mythelene Blue is also used as this is a common measure for the photocatalytic activity of $TiO_2$. The goal is to determine whether ionizing radiation is capable of creating electron hole pairs necessary for photocatalysis in $TiO_2$. The production of these electron hole pairs are critical to proposed production pathway of singlet oxygen.

It is important to note the complexity of the system at hand. Radiolysis produces many comparable

ROS as photocatalytic $TiO_2$ leading to difficulty in determining their origin. Furthermore it is unknown whether $TiO_2$ is able to produce electron hole pairs when irradiated with high energetic photons, leading to photocatalysis. Surface effects may take place on $TiO_2$ regardless of the production of electron hole pairs leading to the production of ROS without being photo activated. The probes used may not be as specific as previously assumed or as sensitive as needed for the doses applied. Because all of these possible processes are connected to each other, a very methodical experimental method is necessary. This will be further discussed in chapter 2 Theory.

## 1.4. Research Questions

This leads to the research questions to be answered in this thesis.

- Are titanium dioxide nanoparticles capable of producing singlet oxygen, when interacting with ionizing radiation?
- Is it possible to uncover the mechanism and dependencies behind the possible production of singlet oxygen and other reactive oxygen species?

# 2

# Theory

This chapter contains more information on the physics and chemistry relevant in this thesis. The physics of electromagnetic (EM) radiation and chemistry of Titanium Dioxide ($TiO_2$) will be discussed. The probes used and variables applied to uncover the ROS present and their underlying mechanisms are also discussed.

## 2.1. Electromagnetic Radiation

Electromagnetic (EM) radiation and photons are physically identical. These photons have an energy depending on their wavelength as can bee seen in equation 2.1, where E is the energy, h Planck's constant, c the speed of light and $\lambda$ the wavelength. When these photons have enough energy to eject an electron from its orbit, this radiation is called ionizing radiation. Below this threshold these photons are non-ionizing electromagnetic radiation which includes radio waves, infrared and visible light. Ionizing radiation includes X-rays and $\gamma$-rays [16]. The distinction between X-rays and γ-rays lies in the origin. X-rays are produced through energy dissipation of electrons while γ-rays are produced through energy dissipation of the nuclei [17].

$$E = \frac{hc}{\lambda} \tag{2.1}$$

### 2.1.1. Interactions of Electromagnetic Radiation with Matter

The wave-particle duality of EM radiation or photons means they can interact both as a wave and a particle. The particle like interactions of interest, which results in ionization and cell death, are photon collisions with electrons in matter. Depending on the mass of the medium and the photon energy, different photon-electron interactions may occur [18]. These effects include the photoelectric-, compton effect and pair production. The region of dominance for each effect is given in figure 2.1.

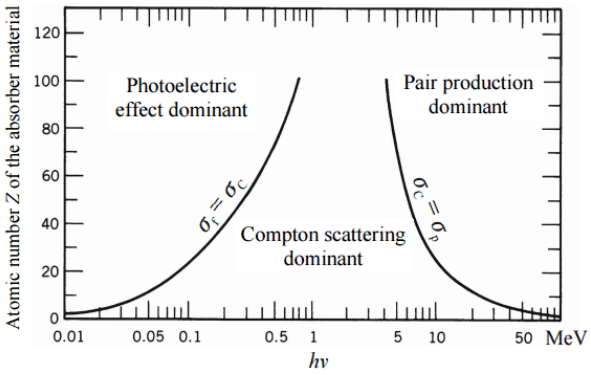


Figure 2.1: The three main photon interactions : photoelectric effect, Compton scattering and pair production. One of these interactions is the dominant effect based on the atomic mass of the medium, Z, and the photon energy, hv. [19]

The mass and energy range used in this thesis result in the photoelectric and Compton effects being dominant.

In the photoelectric effect all the energy of the photon is absorbed by a tightly bound electron. This electron is then ejected from the atom with an energy equal to the energy of the incoming photon minus the binding energy. Electrons with a higher binding energy are more probable to interact with a photon than electrons with a low binding energy. The most tightly bound electrons, with the highest binding energy, are in the K and L shell. The ejection of electrons in the the K and L shell result in vacancies which will be filled by electrons from the outer shell structure with more energy. During this transition the excess energy is dissipated through characteristic X-rays or the ejection of other electrons called Auger electrons.

During the Compton effect the photon collides with a more loosely bound, or free, electron transferring some of its energy. The photon ricochets off the electron under an angle of scatter, θ. This angle also determines how the initial photon energy is divided over the Compton electron and scattered photon [20]. A visual representation of both effects is given in figure 2.2 below.

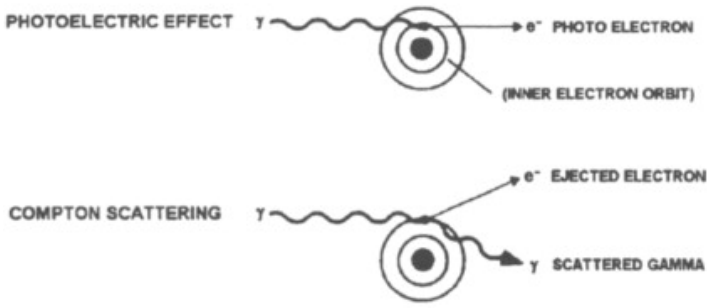


Figure 2.2: A visual representation of the photoelectric effect and Compton scattering [21]

Only a part of the photon energy is transferred in the Compton effect. The energy of a Compton electron depends on the initial photon energy and the angle of scatter. The energy of the scattered Compton electron is given in equation 2.2 and the scattered photon in equation 2.3, where $\alpha = E/m_0c^2$, the energy of the initial photon divided by the rest mass of an electron. The Compton electron will have a maximum energy which is given by equation 2.4. The angle in which the scatter reaction occurs depends on the initial photon energy. The angle favors a narrow forward cone, small angles, for photons with an energy above 511 keV [20]. A visual representation is given in 2.3.

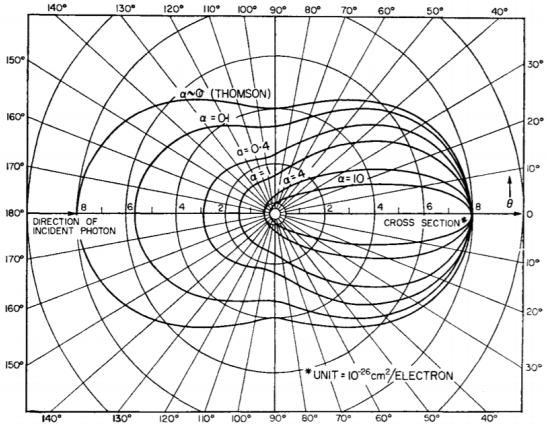


Figure 2.3: The cross section which corresponds to the probability as function of incident photon energy E, where $\alpha = E/m_0c^2$ and $\theta$ the angle of the scattered electron.

$$E_e^c = \frac{E}{1 + \alpha(1 - \cos\theta)} \tag{2.2}$$

$$E_p^c = E - E_{ce} = \frac{\alpha E(1 - \cos\theta)}{1 + \alpha(1 - \cos\theta)} \tag{2.3}$$

$$E_{emax}^c = \frac{E}{1 + 1/2\alpha} \tag{2.4}$$

The contributions of the photoelectric and Compton effect result in the amount of photon interactions in the medium. The probability for an interaction to occur per atom is described by the atomic absorption coefficient and depends on the atomic number of the medium Z and the photon energy. For compound materials the atomic number is slightly different as it is the squared average atomic number, 18.5 for $TiO_2$. The linear absorption coefficient for water, effective Z = 7.4, is given in figure 2.4 where the contributions of each effect are given.

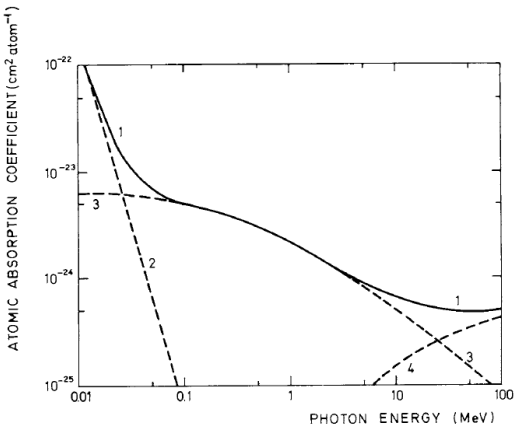


Figure 2.4: Atomic absorption coefficients, cross sections, for water in $cm^2$ per atom as a function of photon energy. The atomic absorptian is the sum of the possible photon interaction. Line 1 is the total absorption, 2 the photoelectric absorption, 3 the compton absorption and 4 the pair production absorption.

To achieve a macroscopic indication for the amount of photon interactions in a medium the linear absorption coefficient is used. The linear absorption coefficient, $\mu$, is the atomic absorption coefficient multiplied with the density of the medium. Lambert's law, equation 2.5, describes the original photon intensity as a function of depth and the linear absorption coefficient, $\mu$. The original photons are lost upon the interactions. Giving an indication for the amount of photons deposited into the medium [22].

$$I = I_0 \exp(-\mu x) \tag{2.5}$$

Here the intensity of the photon beam, I, at a position x is the function of the original intensity, $I_0$, the total linear absorption coefficient, $\mu$, and the position x.

## 2.1.2. Radiolysis

The interactions of ionizing radiation with matter also have chemical effects. The production of new chemical species as a result of ionizing radiation is called radiolysis. The dissociation of electrons lead to charged particles and radicals which can react further creating new chemical species [23].

It is important to note that EM radiation is indirectly ionizing, meaning most of the ionizations occur from a secondary process instead of the initial photon interaction. EM radiation has no charge and therefore does not interact strongly with matter. Charged particles interact heavily with matter as matter consists of positively charged protons and a negatively charged electron cloud. EM radiation can, however, interact through the photoelectric and Compton effect producing an electron. The electron has received an amount of kinetic energy from the collision. This energy will dissipate in the medium through interactions made possible by the charge of the electron. This dissipation causes the majority of excitations and ionizations in the medium [24].

The radiolysis of water is the main interaction of radiation during RT and in this thesis. The important steps are discussed. A visual representation of the steps and time scales in radiolysis is given in figure 2.5. The ionization and production of the electrons and hydrogen ions is called the physical stage which has a duration in the order of $10^{-15}$ seconds. After the physical stage the physicochemical stage starts in which the electron thermalize and becomes hydrated, ionizing other water molecules in the

process. The $H_2O^+$ ions transfer a proton to a neighbouring water atom and the excited water molecule $H_2O^*$ dissociates into an ·OH and H· radical. This stage takes place in the order of $10^{-11}$ seconds. The final stage is the chemical stage in which the products will diffuse and undergo chemical reactions in the medium. These final products include $H_3O^+_{aq}$, ·OH and ·H which are highly reactive and referred to as ROS. Other products which also are significant are hydrated electrons, $e^-_{aq}$, and hydrogen peroxide $H_2O_2$.

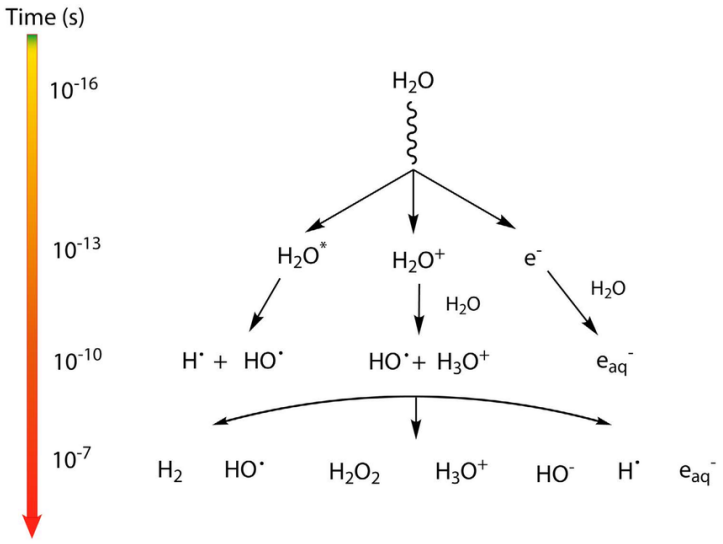


Figure 2.5: Radiolysis productions with the timescale on the left side. When radiation interacts with water the initial products are $H_2O^*$, $H_2O^+$ and $e^-$. From these initial products many follow such as $H_3O^+_{aq}$, $OH$, $e^-_{aq}$, $H$, $H_2O_2$ and $H_2$ [25]

The amount of every product produced in the chemical stage is called the yield. This yield is the amount of molecules produced per 100 eV of radiation absorbed in the water. This value depends on the Linear energy transfer of the radiation [26].

### 2.1.3. Effect Spurs on Physicochemical Stage

The photo- or Compton electron will travel through the medium colliding and ionizing the medium further forming a cluster or spur. These spurs are lines which branch out from the initial electron. High energy electrons do not deviate from their path often implying few collisions. As the electrons lose more of their energy more collisions would occur forming a branch pattern. The ends of these patterns typically are large indistinguishable groups due to the very short branch tracks [27].

The majority of the collisions in these spurs will transfer an energy of less than 100 eV. This is enough energy for further ionisations to take place [28]. The electrons finally thermalize after dissipating their remaining energy and become hydrated.

Radiation with a high linear energy transfer (LET) have a higher potential of cell destruction. This is caused by the ionisation density high LET radiation produces. Higher ionisation densities lead to denser chemical products making double DNA strand breakage more probable resulting in more cell death [29].

Another difference between high and low LET radiation takes place in the physicochemical stage in which the inter-track chemical reactions affect the final products. The tracks in low LET are relatively well-separated clusters of reactive species compared to high LET tracks. The individual spurs in high LET tracks are no longer isolated and can overlap resulting in increased intra-track chemistry. In intra-track chemistry radicals interact with each other creating less free radicals and more molecules at the end of the physicochemical stage [30]. After $10^{-7}$ seconds the spur expansion is complete and the reactive species that remain distribute homogeneously in the medium. The g-values relate to the reactive species at the end of the spur expansion ready to diffuse. The LET for 1 MeV photons from a

Cobalt-60 source for example is 0.3 keV/$\mu m$ while X-rays with an energy of 200 keV have a LET of 1.7 keV/$\mu m$ [31]. This means more free radicals survive the physicochemical stage when using X-rays compared to $\gamma$-rays from the Cobalt source.

## 2.2. Titanium Dioxide Nanoparticles

The relevant mechanisms of $TiO_2$ NPs are discussed in this chapter. This includes its photocatalytic properties, surface effect and crystalline structures. Also a summary is given on the relevant interactions of irradiation with gold NPs as this is a much more researched subject than $TiO_2$ NPs.

## 2.3. Photocatalytic Properties of $TiO_2$

$TiO_2$ is a commonly used photocatalytic NP. $TiO_2$ catalyses a process by absorbing light. Light absorption of the correct energy, around 3.2 eV, results in the creation of electron-hole pairs [32]. An electron from the valence band is excited towards the conduction band. The electron-hole pair generate free radicals through reductive and oxidative reactions. These radicals are among the ROS produced in radiolysis, thereby potentially catalysing cell damage. A visual representation of photocatalytic $TiO_2$ is given in figure 2.6 [33].

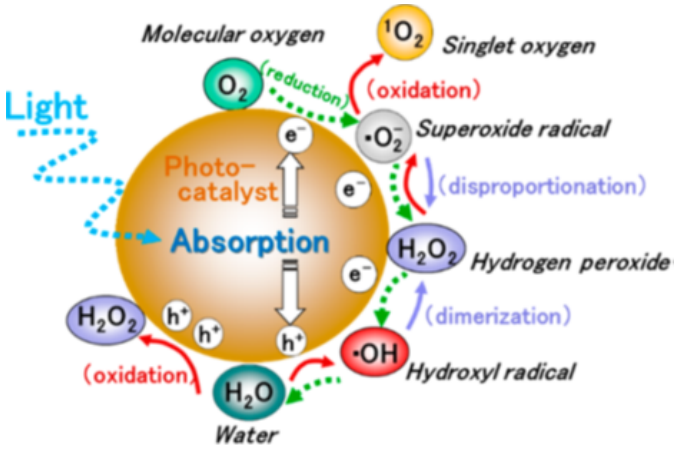


Figure 2.6: An overview of the Reactive Oxygen Species that are produced in the photocatalysis of $TiO_2$ in water. Upon the absorption of light an electron from the valence band is excited towards the conduction band, creating an electron hole pair. The electron can reduce oxygen into a superoxide radical, $\cdot O_2^-$, and the hole can oxidize water into a hydrogen, ·H, and hydroxyl radical, ·OH. Further reactions are facilitated by the $TiO_2$ surface. The most important is the singlet oxygen, $^1O_2$ production by oxidizing a superoxide radical [34].

Other reactions resulting in different radicals than ROS produced in radiolysis are also facilitated by $TiO_2$. Two very important reactions which occur are the oxidation of hydrogen peroxide, $H_2O_2$, and reduction of oxygen both resulting in a superoxide radical, $\cdot O_2^-$. The superoxide radical can then oxidize into singlet oxygen, $^1O_2$. These reactions are also given visually in figure 2.6. $H_2O_2$ can also be reduced creating two hydroxyl radicals, ·OH, competing for the conduction band electrons with the reduction of oxygen resulting in superoxide radicals. However, the reduction of oxygen is more efficient and likely to occur in aqueous solutions than the reduction of hydrogen peroxide [35].

The decomposition of $H_2O_2$ remains important as it leads to hydroxyl radicals, ·OH, which are adsorbed on the surface and can act as trapped holes. Trapped holes are holes which have transported to surface hole trap sites, able to oxidize molecules. The ability to oxidize is of special importance as the production of singlet oxygen is expected to be the result of oxidizing a superoxide radical. Singlet oxygen, $^1O_2$, is believed to play a major part in the damage created to living cells by ROS [36] [37].

The difference between molecular oxygen and singlet oxygen lies in the electron configuration. The ground state is characterized by a triplet spin state, $X^3\Sigma_g^-$, while excited singlet oxygen is characterized by the singlet states, $a^1\Delta_g$ and $b^1\Sigma_g^+$. The most common singlet state is $a^1\Delta_g$ as $b^1\Sigma_g^+$ can efficiently

converse into the other. These electron spin configurations are also visible in figure 2.7. The spin configurations of the singlet state are highly reactive resulting in a short lifetime of the singlet oxygen [38].

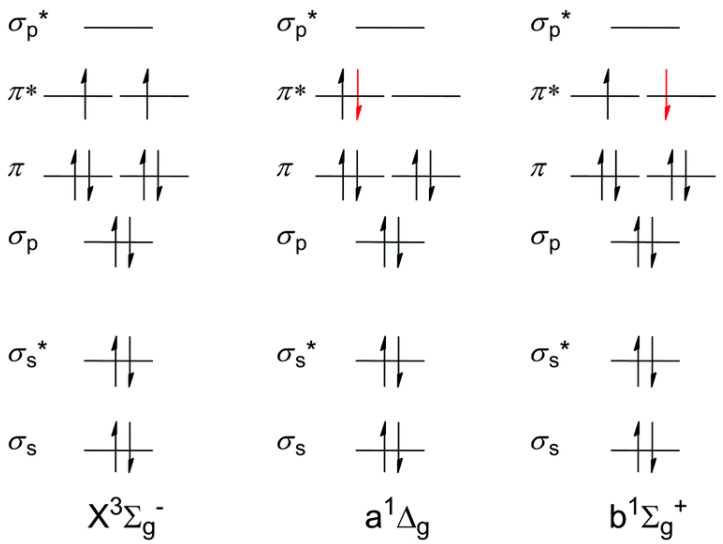


Figure 2.7: Three different electron spin states of dioxygen, $O_2$. The triplet state $X^3\Sigma_g^-$ and the two singlet states $a^1\Delta_g$ and $b^1\Sigma_g^+$. When talking about singlet oxygen the $a^1\Delta_g$ is referred to [38].

Although there are some indications $^1O_2$ is formed during radiolysis, the process which occurs during RT, the majority is expected to be created through the photocatalytic activity of $TiO_2$ [39].

The production $^1O_2$ by $TiO_2$ is the reason of interest for the application of NPs in combination with RT. However it is unknown whether $TiO_2$ is able to produce $^1O_2$ when irradiated with X-rays. The band gap energy needed for $TiO_2$ to form electron-hole pairs is approximately 3.2 eV. Photon energies used in radiation therapy vary from 100 keV up to 25 MeV depending on the tumor depth [40]. This discrepancy leads to the research question.

### 2.3.1. Surface Effects

Other reactions apart from photocatalytic reactions take place on the surface. The most important of which can also result in the oxidation of a molecule. The reactions able to oxidize molecules have been summarised in figure 2.8.

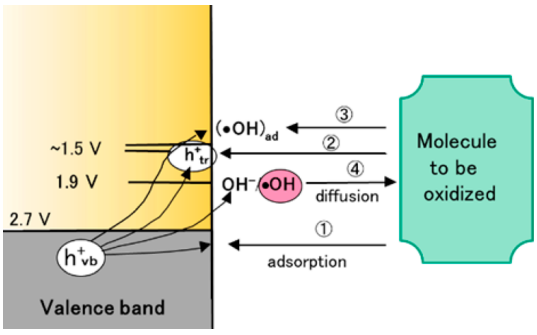


Figure 2.8: The oxidation reaction facilitated by $TiO_2$ NPs. 1, direct oxidation by hole. 2, hole first transports to trapsite at surface before direct oxidation. 3, oxidation of surface hydroxyl group resulting in hydroxyl radical which is adsorbed at the surface. 4, release and oxidation by adsorbed hydroxyl radicals produced by ionizing radiation or pathway 3 [34].

The excitation of an electron leads to a hole, which is transported towards the surface of the $TiO_2$ NP. Here it can interact in different ways, all resulting in an oxidative reaction. Pathway 1 is the direct oxidation of a molecule by a hole. In pathway 2 the hole stabilizes on the titanium surface to become a

trapped hole from which it can oxidize a molecule at the surface. Pathway 3 is the production of an adsorbed hydroxyl radical due to the oxidation of a surface hydroxyl group. Pathway 4 is the oxidation reaction facilitated by the adsorbed hydroxyl radical. The adsorbed hydroxyl radicals generated through pathway 3 or radiolysis detach from the surface and can oxidize a molecule away from the surface. The adsorbed hydroxyl radicals and trapped holes perform the same function and have similar properties resulting in difficulty in identifying the origin of oxidation [34].

These different oxidation pathways are important as the decomposition of $H_2O_2$ on the surface leads to adsorbed hydroxyl radicals, capable of oxidation. This decomposition process has an Arrhenius energy of $37 \pm 1$ kJ $mol^{-1}$, which means the decomposition occurs spontaneously at room temperature [41]. What is interesting about this process is the oxidizing properties of the hydroxyl radicals can add or even over compete with the photo activated catalytic properties of $TiO_2$.

The adsorption of hydroxyl radicals on the $TiO_2$ surface also result in a decreased band gap energy. This decrease in energy band gap allows lower energies to cause electron excitations towards the conduction band [42]. Facilitating the photocatalytic effect to occur for lower energy photons than usual [43]. This promotes the production of superoxide radicals, $\cdot O_2^-$, by $TIO_2$ under irradiation as lower photon energies are required [44]. The oxidation by adsorbed hydroxyl radicals can even compete with the oxidative capabilities of the photocatalyst. High $H_2O_2$ concentrations can create a sufficient amount of adsorbed hydroxyl radicals to perform catalytic functions without the $TiO_2$ being photo activated [45].

Although the needed $H_2O_2$ concentration for spontaneous catalysis, 4.9 M, will not be reached in this thesis, the decreased bandgap and increased superoxide production are of interest [45].

### 2.3.2. Rutile and Anatase

The photocatalytic activity also depends on the crystal structure of $TiO_2$. Two crystal structures exist, Anatase and Rutile. A visual representation is given in figure 2.9, where the left structure is anatase and the right rutile. The surfaces and their miller indices are also given.

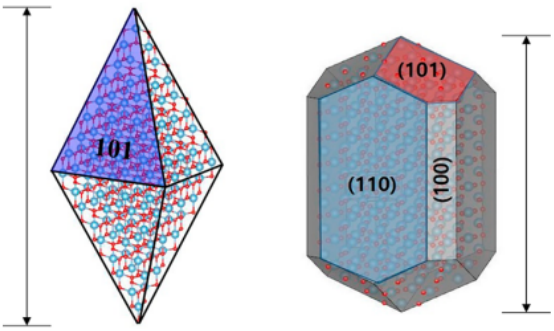


Figure 2.9: A visual representation of Anatase (left) and Rutile (right) $TiO_2$ crystaline structures. The important surfaces and their miller indices are also represented [46].

Anatase is the more photo active crystal structure. An explanation for the difference in this activity lies in the thermodynamic stability of certain surfaces which produce more hydroxyl radicals upon irradiation. It was found that the oxidative properties through methanol oxidation of single-crystal anatase (101) surfaces are greater than all single-crystal rutile surfaces. An indirect measurement of hydroxyl production resulted in comparable photocatalytic activity of rutile (001) and anatase (101) surfaces. However rutile (001) is not thermodynamicly favourable while the other, less photo active, surfaces are. This gives an indication why anatase in more photo active from a structural point of view [47].

The proposed reason why rutile $TiO_2$ is less photoactive lies in the surface structure. The inter atomic distance between the titanium molecules is smaller in the case of rutile $TiO_2$. This allows for a Ti-OO-Ti surface structure to arise. It is proposed that because photoinduced electrons are used to create these Ti-OO-Ti surface structures, less photoinduced electrons are present to perform photocatalytic functions, decreasing the overall photoactivity [48][32].

The combination of anatase and rutile results in the best photocatalytic activity, however, there is no consensus as to why. The leading theory is based on the interaction of the different band gaps [34].

### 2.3.3. Nanoparticles And Radiation

Research on the interaction of $TiO_2$ NPs with irradiation has shown an increase in ROS produced dependent on the $TiO_2$ NPs concentration and the energy of photon irradiated, favouring high concentrations and low keV photon energies [14]. The origin for this production was not concluded but electron hole production resulting in oxidative and reductive effects on the $TiO_2$ surface are expected. Further research on the origin of the increased yield gave different results. Two papers claim different results in the increased production of $H_2$ as a result of the NP presence when irradiated. Both state that ionizing radiation is capable of creating electron hole pairs and that the oxide surface interacts positively in the production of $H_2$. However one paper claims that this is not the case for the oxide surfaces of $TiO_2$ NPs [49]. Another paper did find an increase in $H_2$ as the result of $TiO_2$ NP presence, they used kGy which might explain the difference in conclusions found [50]. No conclusions can be drawn from literature apart from the importance of the oxide surface and the production of electron hole pairs.

Plenty of research has been done on the interactions of gold nanoparticles and photon irradiation. Although gold is different from $TiO_2$ due to a higher atomic weight, Z, some insights may be gathered.

An important insight from this literature is the discrepancy of local radiation effects versus macroscopic radiation effects. The dose distribution is very inhomogeneous, with very high doses around NPs compared to the rest of the medium. These high doses around the NP are caused by Auger electrons ejected as a result of the photoelectric effect. During the photoelectric effect, an inner shell electrons is ejected leaving a vacancy. This vacancy will be filled by outer shell electrons. The outer shell electron must lose some energy in order to fall into a lower electron orbital. This process results in a X-ray or the excitation or ejection of another outer shell electron. Each falling electron creates new vacancies allowing for a possible cascading effect. These electrons are called Auger electrons. A single inner shell electron ionisation can result in a multitude of Auger electrons. Auger electron typically have a low energy, meaning they can only interact near the surface of the NP. This leads to the very local effect of dose enhancement [29][51]. A visual representation of these Auger cascades and the dose given per distance from the NP surface is given in figure 2.10.

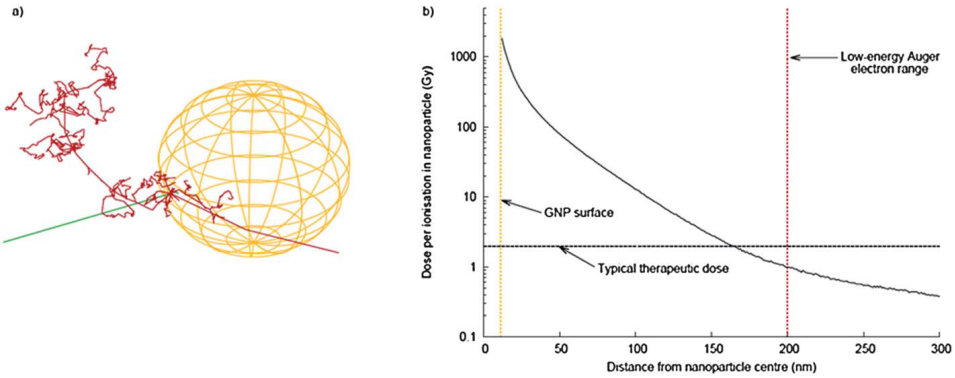


Figure 2.10: Illustration of the interaction of a high energy photon and a gold nanoparticle, simulated using Geant4. Picture a indicates the initial photon in green and the ejected Auger electrons in red. Picture b indicates the calculated dose resulting from a single ionisation event as a function of distance from the NP [29].

The photoelectric effect is dominant around photon energies of 80 keV in combination with gold. Some research has shown similar gold NP ionisation rates and comparably large doses near the NPs when using photon with an energy of a few MeV. This is explained as the result of high energy secondary electron from Compton scattering with the NP or medium [52].

The production of hydroxyl radicals due to the irradiation of gold NPs has also been reported. It was observed that the production increased, which could not be attributed towards the increased energy deposition due to linear attenuation. The increased production is attributed to the water-nanoparticle interface. This production is dose rate dependent, declining with rising dose rates. This dependency is explained with the analogy of recombinations occurring in heavy ion tracks. A greater amount of hydroxyl radicals produced will result in a bigger chance of recombination decreasing the overall production [11].

## 2.4. Experimental Approach

The effect of ionizing radiation on $TiO_2$ NPs will be measured using probes in this thesis. Samples containing a probe are prepared. Half of the samples get $TiO_2$ added to them leaving the other half as a control group. All samples are then subjected to the same irradiation conditions. The samples are centrifuged after irradiation in order to remove the $TiO_2$ from the solution. The remaining probe is then measured, leaving the $TiO_2$ presence during irradiation as the only variable.

Two different radiation sources are used, a X-ray source and a Cobalt-60 source. The X-ray source emits a range of photon energies of which the peak energy and the dose rate can be set. Energies of the X-ray source vary from 60 keV towards 300 keV and the dose rate is in the order of a few Gy/h. The Cobalt source only emits photon at 1.17 and 1.33 MeV. Two sources are available of which the dose rate decays over time. The high dose rate source is the Cobalt 220 which had a dose rate around 10 Gy/min at the time of the experiments and the low dose rate source is the Cobalt 200 which had a dose rate around 0.7 Gy/min.

The probes used and the variables applied will be discussed in the chapters below. The impact of each variable is explained in order to uncover the mechanisms at play.

### 2.4.1. SOSG

Singlet Oxygen Sensor Green (SOSG) reagent is a fluorescent probe made by the company Invitrogen. The probe is marketed as highly selective towards singlet oxygen and not towards superoxide or hydroxyl radicals. The exact structure is not public knowledge but based on the absorption spectrum the probe consist of a fluorescein and anthracene moiety. The reaction with singlet oxygen renders the probe fluorescent when illuminated with photons of 504 nm as it can no longer dissipate the energy of the excited electron through internal conversion as is visible in figure 2.11 [53].

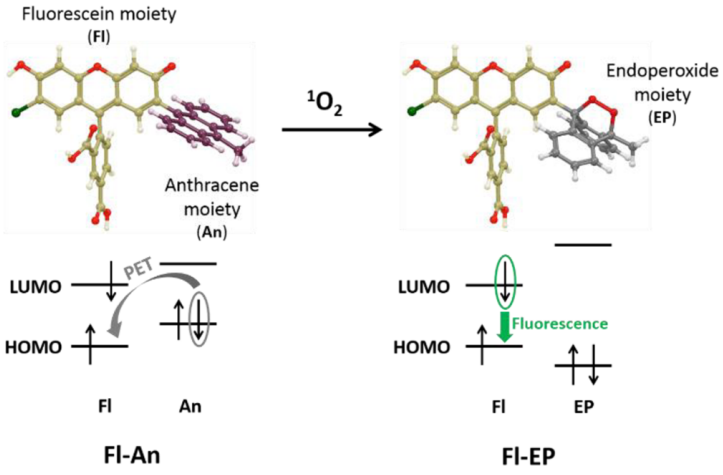


Figure 2.11: The shift from the Anthracene moiety into the Endroperoxide moiety upon reacting with singlet oxygen. The LUMO, lowest unoccupied molecular orbital, and HOMO, highest occupied molecular orbital, of these moieties are also given. The shift in these molecular orbitals renders the probe fluorescent [53].

The interaction of SOSG with singlet oxygen changes the anthrascene (An) moiety into an endoperoxide (Ep) moiety. The SOSG-EP has different characteristics than normal SOSG, which is SOSG-An. The first is a rise in fluoresence for SOSG-EP at 530 nm with an activation wavelength of 504 nm.

The second is a shift in the UV-Vis absorbance of the SOSG/SOSG-EP solution. The shift in UV-Vis absorbance spectrum is a noticeable drop at 258, 376, 396 and 507 nm [54]. An example of the rise in fluoresence, dotted line, and the decrease in absorbance, solid line, is given in figure 2.12.

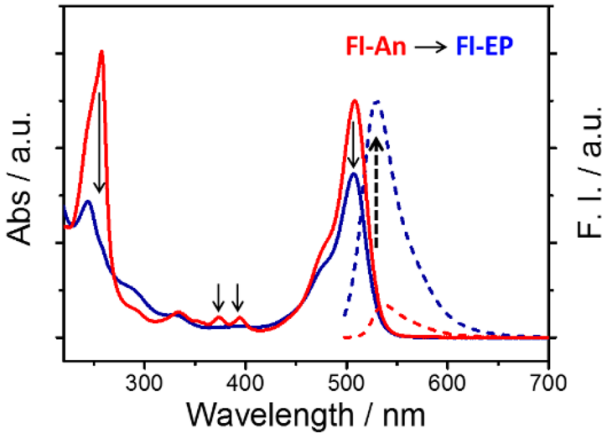


Figure 2.12: Absorption spectra (solid line) and fluorescent spectra of standard SOSG (Fl-An) and SOSG-EP (Fl-EP) which has reacted with singlet oxygen. The black arrows indicate the transition from SOSG towards SOSG-EP over time [53]

Because SOSG is expected to be highly specific towards singlet oxygen, variables are targeted which may influence the production of singlet oxygen. These include the dose rate, photon energy, surface effect, free oxygen presence and the presence of radicals. For each of these the possible relation is discussed below to explain the possible production dependence.

**Dose Rate**
The dose rate is an important variable for two reasons. The first being an indicator towards chemical enhancement and the second indicating if comparisons can be made between radiation sources regardless of their dose rate. Chemical enhancement is a term which describes the enhancement of a signal, in this case SOSG fluoresence, as a result of a secondary reaction facilitated by the presence of $TiO_2$ [6]. This secondary reaction is not specified and may use chemical species created during radiolysis. The amount of species produced during radiolysis therefore could be a variable for the amount of enhanced signal. The amount of species produced by radiolysis at a given moment is dependent on the dose rate. A small dose rate, leading to a low production of species per time, may fully undergo the secondary reaction while a high dose rate, leading to a high production of species per time, may lead to the reaction being saturated. Apart from providing some insight in the mechanism of singlet oxygen production, the dose rate dependence also has a practical goal. There are three sources for photon irradiation available, two being different cobalt sources and the third an X-ray tube. The two cobalt sources have the same photon spectrum but a different dose rate while the spectrum emitted by the X-ray tube can be varied. It is important to know whether data acquired from different radiation sources can be compared or not.

**Photon energy**
Variations of the photon energy are applied in an effort to gain an understanding whether the production of singlet oxygen is favourable in certain energy ranges. This information is useful as it may reveal the mechanisms of singlet oxygen production as well as information towards possible practical implementation. The mechanism could be linked to physical enhancement, a rise in signal due to increased energy absorption, which is photon energy dependent. If $TiO_2$ is used as a dose enhancing agent it is important to know which photon energies lead to the best result.

Two different experiments were conducted. The first being a comparison between two different X-rays spectra with the same dose rate. The second being a comparison between an X-ray spectrum and gamma's originating from a $^{60}$Co source.

**Surface effects**

A chemical reaction of $TiO_2$ resulting in singlet oxygen should occur on the surface of the NP. In an attempt to exclude any chemical reaction $TiO_2$ NPs with an inert layer were purchased. In order to have a correct comparison uncovered anatase NPs were also purchased. The goal of the experiments was to prove that chemical reaction occur on the surface of $TiO_2$ upon photon irradiation.

**Aerobic and Anaerobic environment**
The presence of free oxygen in a sample is expected to be necessary for the production of singlet oxygen. The production of superoxide radicals, necessary in the production of singlet oxygen, can be stopped. The superoxide radicals have two origins the first being the reduction of free molecular oxygen and the second being the oxidation of hydrogen peroxide on the surface of $TiO_2$. Removal of free oxygen in the sample should lead to a decreased superoxide as oxygen can no longer be reduced and therefore a decreased singlet oxygen production. The oxidation of hydrogen peroxide remains possible.

**Radical Presence**
The production of singlet oxygen is expected to occur with an intermediate step, namely a superoxide radical. Removal of these radicals should lead to a stop in singlet oxygen production. The following experiments use radical scavengers in order to remove superoxide radicals among others from the solution. The radical scavengers which are used are a HEPES buffer and ascorbic acid, better known as vitamin C.

### 2.4.2. Mythelene Blue

Mythelene Blue (MB) is often used as an indicator for the photocatalytic activity of $TiO_2$. The radicals produced during photo excitation can oxidize MB resulting in a measurable degradation [55]. The degradation is measured using UV-Vis absorbance spectrum. The degradation is seen as the complete loss of absorbance with the important peaks at 292 and 663 nm, as can be seen in figure 2.13 [56].

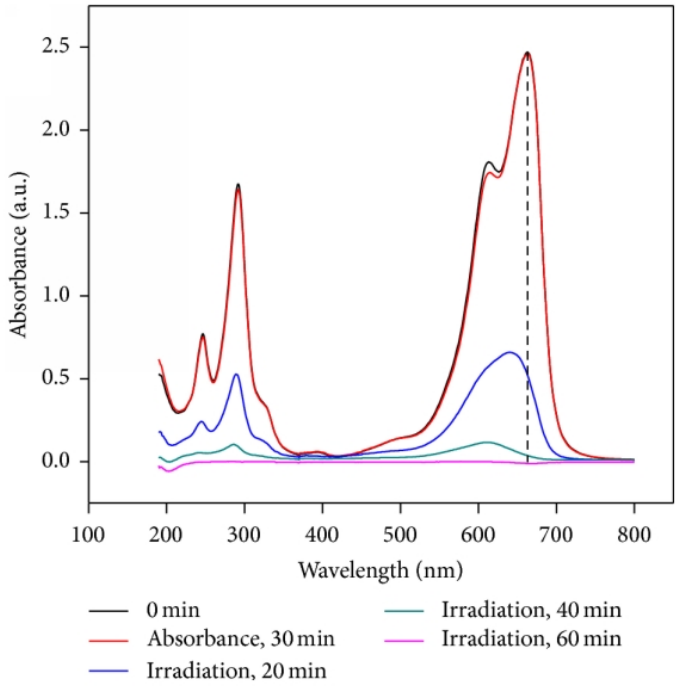


Figure 2.13: A visual representation of the degradation of mythelene blue, measurable as a decline in UV-Vis absorbance, as a result of the photocatalytic activity of $TiO_2$ [56].

The production of singlet oxygen is expected to be the result of the oxidation of superoxide radicals. Measurements on the amount of oxidization as a result of photocatalytic $TiO_2$ can provide insight in the production method. When variables are applied which quench the SOSG signal also result in a diminished MB degradation, a correlation between the photocatalytic effect and singlet oxygen production is

likely.

Firstly the degradation of MB as a result of $TiO_2$ exposed to ambient light and irradiation is measured. Afterwards variables are applied in effort to promote or demote the production of ROS or electron hole pairs. These variables are discussed below.

**Anaerobic Conditions**
Although the production of electron hole pairs is independent of the presence of oxygen in the solution, the degradation may be caused by ROS instead of the direct interactions with $TiO_2$. The goal is to gain an understanding if ROS or direct interactions of $TiO_2$ drive the degradation of MB.

**Surface Effects**
The adsorption of hydroxyl radicals on the surface of $TiO_2$ perform the same function as trapped holes. The adsorbed hydroxyl radicals can oxidize other molecules but can also result in a decreased band gap energy possibly allowing more electron hole pairs to be formed. The presence of hydrogen peroxide increases the amount of adsorbed hydroxyl radicals on the surface. The goal is to gain an understanding if the amount of hydrogen peroxide produced during radiolysis is enough for these surface effects to play an important role in the degradation of MB.

**Radical Scavenger**
Apart from removing oxygen from the solution, ROS can also be actively quenched. The quencher used is HEPES. The goal is to gain an understanding if the degradation of MB is driven by ROS.

# 3

# Methods & Materials

This chapter discusses the materials, radiation sources and bubbling techniques used in more detail.

## 3.1. Materials

**$TiO_2$**

$TiO_2$ NPs were purchased, the P25 from Sigma Aldrich, the anatase and silica covered NPs from Nanostructured and Amorphous Materials Incorparated. The P25 had an average particle size of 20 nm and is about 15 percent anatase and 85 percent rutile. The specific surface was not given. The uncovered NPs had an average particle size of 20 nm, specific surface area of 5 $m^2/g$ and a crystalline structure of 80-90 % anatase and 10-20 % rutile [57]. The silica covered NPs had an average particle size of 20 nm, specific surface area of 40 $m^2/g$ and a crystalline structure of 80-90 % anatase and 10-20 % rutile [58].

Samples were prepared by weighing the desired amount of $TiO_2$, usually 5 mg, and adding 10 ml of MilliQ resulting in a $TiO_2$ solution of 0.5 g/l. The solutions were placed in the ultrasonic bath for half an hour before use to ensure an even dispersion.

**SOSG**

The probe SOSG was acquired from Invitrogen in sets of 10 vials each containing 100 $\mu$g. Stock solutions were prepared by dissolving the content of a SOSG vial in methanol (33 $\mu$L). The dissolved contents of the SOSG vial were diluted with 67 $\mu$L of MilliQ after which the solution was transferred to a glass vial wrapped in aluminium foil to block any light from reaching the solution. The SOSG vial was washed 2 times with 200 $\mu$L of MilliQ to ensure all contents are extracted. The final stock solution was further diluted with 16 mL of MilliQ, resulting in the final 16.5 mL, 10 $\mu$M SOSG solution [59].

The fluorescence of the SOSG probe was measured using a fluorescence spectometer. The fluorescent emission spectrum was measured from 600 nm down to 510 nm in steps of 1 nm after photon excitation at 504 nm. The UV-Vis absorbance of SOSG was measured from 600 nm down to 240 nm in steps of 1 nm using a UV-6300PC Double Beam spectrophotometer. The samples were centrifuged for 30 minutes before measurements to ensure the $TiO_2$ settled on the bottom of the vial and only the SOSG solution was measured.

The final samples contained a 0.5 ml of the SOSG stock solution and 0.5 ml of water or 0.5 ml of the $TiO_2$ stock solution. Resulting in samples containing a 5 $\mu$M SOSG solution with or without an added $TiO_2$ concentration of 0.25 g/l.

**Mythelene Blue**

Mythelene Blue (MB) was purchased from J.T. Baker now known as Avantor. To arrive at a concentration of 0.02 g/l a solution with a concentration of 0.5 g/l was prepared using the a weight scale. This solution was diluted 25 times resulting in a 0.02 g/l solution.

The UV-Vis absorbance of MB was measured from 770 nm down to 200 nm in steps of 1 nm using a UV-6300PC Double Beam spectrophotometer. The samples were centrifuged for 30 minutes before measurements to ensure the $TiO_2$ settled on the bottom of the vial and only the MB solution was measured. The solutions of the MB were checked and possibly diluted before measuring to ensure the 0 Gy sample set had an absorbance below 1 as this is the most accurate region [60].

The final samples contained a 0.5 ml of the MB stock solution and 0.5 ml of water or 0.5 ml of the $TiO_2$ stock solution. Resulting in samples containing a 0.1 g/l MB solution with or without an added $TiO_2$ concentration of 0.25 g/l.

**Radical Scavengers**
Two different radical scavengers were used. A HEPES buffer solution, pH = 7.4 10 mM, and an ascorbic acid solution, pH 3.6 5mM.

The radical scavengers were used to create $TiO_2$ stock solutions. Final samples remain the same for both SOSG and MB, using $TiO_2$ dissolved in the radical scavenger.

## 3.2. Radiation sources

**X-ray**
The X-ray source used was a Phillips MCN 321 X-ray tube with a Wolfram anode. The source emits an X-ray spectrum with a variable peak energy, maxing out at 320 keV. The X-ray spectrum used was set at a peak energy of 185 keV, 18 mA with a filter containing 3.9 mm thick aluminum and 5.01 mm thick copper plating, resulting in a dose rate of 6.4 Gy/h. Dose rate measurements are possible for this filter as the ionisation chamber has been calibrated.

**Cobalt 60**
Two different gamma sources were used ($^{60}$Co sources). The older source was the Cobalt 200 source which had a dose rate around 0.8 Gy/min at the time of measurement. The more recent source was the Cobalt 220 which had a dose rate around 10 Gy/min at the time of measurement. The dose rates of these sources were tabulated per date.

## 3.3. Oxygen Removal

**Nitrogen Bubbling**
The solutions were placed in a glass vial and sealed with a rubber cap. A needle was pierced through the cap allowing Nitrogen to flow into the solution. A second needle was placed freely into the cap allowing an nitrogen flow to occur. A magnetic stirrer was added to increase the exchange of oxygen and nitrogen. The solutions were bubbled continuously over a period of 24 hours. During this time some of the water in the solution would evaporate. A third vial of water was also bubbled, to be used to return to the original concentrations of the $TiO_2$, MB or SOSG solution.

**Argon Bubbling**
The bubbling setup with Argon did not make use of rubber caps. A glass pipette was connected to the argon tank which was placed in an open Erlenmeyer, leaving the sample exposed to the atmosphere at all times. The Argon flow was kept in the sample for a maximum of 30 minutes. During this time no noticeable evaporation took place.

# 4

# Results & Discussion

## 4.1. Singlet Oxygen Production

The interaction of $TiO_2$ NPs with ionizing radiation is expected to result in the production of ROS possibly including singlet oxygen. The possible interactions of a NP with ionizing radiation and the chemical reactions facilitated by $TiO_2$ are shown once more in figure 4.1 for clarity's sake. The oxidation of superoxide radicals resulting in singlet oxygen is a chemical reaction facilitated by $TiO_2$, indicating the enhancement to be chemical in nature, pathway C in figure 4.1.

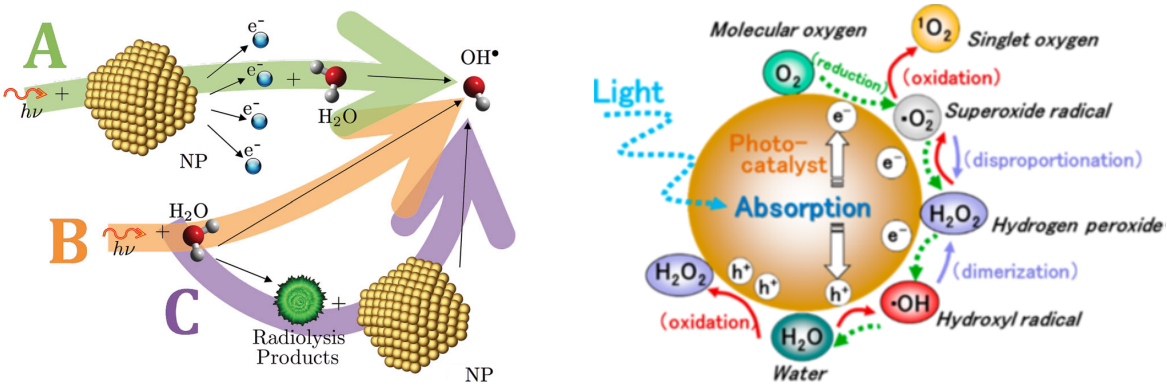


Figure 4.1: The possible interactions of ionizing radiation with NPs resulting in the enhancement of hydroxyl radicals, ·OH, and the chemical reaction facilitated by $TiO_2$. Pathway C of the interactions include the photo catalytic properties of $TiO_2$. Although pathway C says radiolysis products + NP, reaction of the NP with water are also included.

In order to detect singlet oxygen the probe Singlet Oxygen Sensor Green (SOSG) used. SOSG is a commercially available probe which is claimed to be highly specific towards singlet oxygen. The response in fluorescence and UV-Vis absorbance of the probe to singlet oxygen, visible in figure 4.2, is used as an indicator for the amount of singlet oxygen present. Only the peak values at 510 nm from the fluorescent intensities will be shown in the results as bar plots for different received doses.

In the past SOSG has shown to be sensitive to radiation. The sensitivity is expected, but not proven, to be a response to hydrated electrons based on research performed by H. Liu and P. Carter [61]. This possible sensitivity allows the impact of physical enhancement, pathway A in figure 4.1, to cause a significant increase in signal response, as the production of electrons is enhanced during physical enhancement resulting in increased local radiolysis and hydrated electrons. This could lead to a rise in fluorescent signal while no singlet oxygen is produced.

In order to identify the origin of the response by SOSG, variables are applied in effort to uncover the mechanisms at play and the type of enhancement resulting in an increased fluoresecent SOSG signal. The variables and their results are discussed in the following sections.

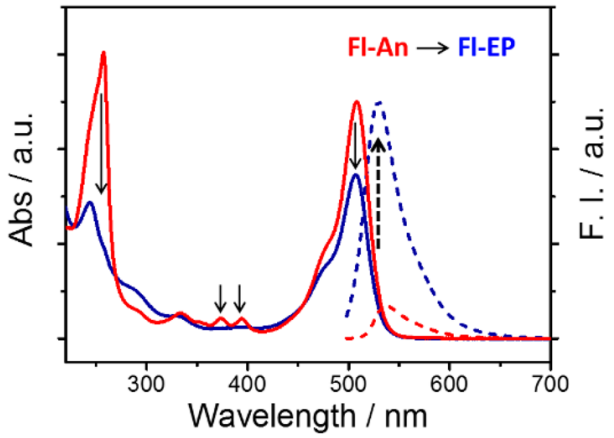


Figure 4.2: Absorption spectra (solid line) and fluorescent spectra of standard SOSG (Fl-An) and SOSG-EP (Fl-EP) which has reacted with singlet oxygen. The black arrows indicate the transition from SOSG towards SOSG-EP over time [53].

### 4.1.1. Fundamental Properties of SOSG

Some fundamental properties of SOSG that came to light over the course of the experiments. These properties indicate the limitations of the probe and determine which results can be compared.

The first property which came to light is that each batch of SOSG has a different fluorescent intensity. This inconsistency includes both the initial fluorescence before exposure to irradiation as well as the rise in fluorescence to the same irradiation conditions. Therefore it is not possible to directly compare experiments performed with different SOSG batches but possible to compare within the same batch.

The second property is the probe's sensitivity to ambient light. The probe itself is not sensitive to light exposure whereas SOSG in combination with $TiO_2$ is. All experiments were performed in black plastic vials and light exposure was kept to a minimum.

The final property is the inability to consistently measure the shift in UV-Vis absorbance from SOSG-An towards SOSG-EP. The UV-Vis spectra of the SOSG solutions were measured to ensure the increase in fluorescence occurred in combination with a shift in absorbance towards SOSG-EP. The expected shifts are a drop at 258, 376, 396 and 504 nm as can be seen in figure 4.2. No shift however has been consistently measured. The presence of $TiO_2$, even after removal through centrifugation, has an impact on the SOSG UV-Vis absorbance. The peak absorbance at 504 nm, which should be the most noticeable drop, shows fluctuations as a function of dose. The samples that have not been in contact with $TiO_2$ also show no consistent shifts in the UV-Vis absorbance. An initial drop in UV-Vis is measured after being exposed to irradiation after which the drop halters while the fluorescence continues to increase with dose. This means no clear link between the rise in fluorescence and a decline in UV-Vis absorbance was found.

The complete absorbance spectra in which the fluctuating UV-Vis absorbance as a result of the presence of $TiO_2$ can be seen in the appendix in figure A.1. Figure A.3 shows the the peak absorbance at 504 nm as a function of dose to clearly illustrate the fluctuations. The absorbance spectra of SOSG that have not been in contact with $TiO_2$ NPs, in which a clear initial drop is visible after which the decline halters is visible are also given in the appendix. The complete absorbance spectrum is given in the figure A.2 and figure A.4 highlights the amount of absorbance at the 504 nm peak.

### 4.1.2. Dose Rate

The dose rate is an important variable as it is an indicator towards chemical enhancement. As mentioned, pathway C consists of many different chemical reactions. A discrepancy between these reactions is whether they occur using products created during radiolysis. A dependence of dose rate is a clear indicator that a chemical reaction utilising products from radiolysis occurs.

Firstly the dose rate dependence when using the X-ray source was looked into. Samples containing $TiO_2$ NPs (0.25 g/l) received a dose of 1 Gy with a peak photon energy of 140 keV. The dose was administered with a rate of 2, 1 and 0.5 Gy/h. The results are given in figure 4.3.

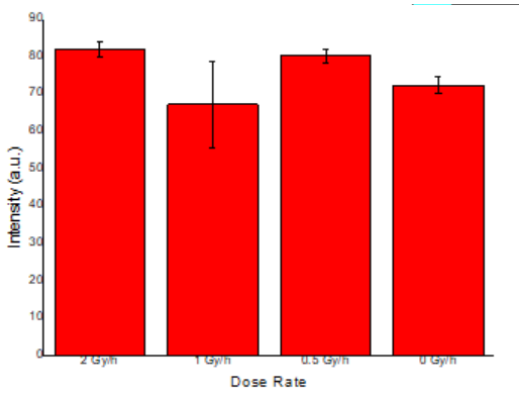


Figure 4.3: Fluorescent intensity of a centrifuged SOSG (5 $\mu$M) and $TiO_2$ (0.5 g/l) solution irradiated with a 140 kVp X-ray spectrum. Samples received 1 Gy with a variable dose rate, from left to right 2, 1 and 0.5 Gy/h, and a control sample which received no radiation. Standard deviation applied based on variations between samples.

Although the increase in fluorescence is minimal no significant differences between the different dose rates are apparent. The origin for the increased uncertainty in the case of a dose rate of 1 Gy/h is unknown. Nonetheless the similarity of the results for a dose rate of 2 and 0.5 Gy/h, leads to the conclusion that no dose rate dependence is apparent when irradiating SOSG in the presence of $TiO_2$ with a 140 kVp X-ray spectrum.

The same variables were applied to a SOSG solution without $TiO_2$ NPs present. These experiments resulted in a small rise in intensity compared to the uncertainty, such that no conclusion could be made. The results are given in the appendix in figure A.5. To overcome this uncertainty the received dose was increased from 1 Gy toward 3 Gy. Limited exposure times required an increase in peak energy resulting in a higher dose rate, allowing higher doses to be reached. The results from this repetition were inconclusive once more and also given in the appendix in figure A.6. The filter was removed from the X-ray tube for the final attempt. As a result the dose rate was unknown. However the dose rate remained linear with the amperage. This allowed the dose rate to be set at full capacity, half and a quarter capacity. The results are shown in figure 4.4

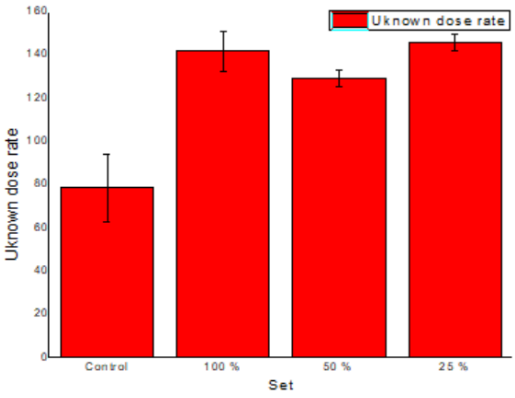


Figure 4.4: Fluorescent intensity of the SOSG (5 $\mu$M) solution irradiated with a 185 keV peak energy X-ray spectrum. Samples received an unknown variable dose rate, from left to right 0, 25, 50 and 100%. Standard deviation applied based on variations between samples.

Similarly to the case with $TiO_2$ NPs present, no clear dose rate dependency is visible. The deviation in the case of the 50% dose rate is not significant enough to deviate from the conclusion that in the

case of low X-ray energies the amount of fluorescence is not dose rate dependent regardless of the presence of $TiO_2$.

The experiments were repeated for the two $^{60}$Co sources. The difference in dose rate between these sources varies per day as they decay. The $^{60}$Co 200 source is the older source which has a dose rate of 0.728 Gy/min and the $^{60}$Co 220 source 10.08 Gy/min at the day of the experiment. The results for both with and without $TiO_2$ NPs as well as the two $^{60}$Co sources are visible in figure 4.5 as a bar plot and a linear plot.

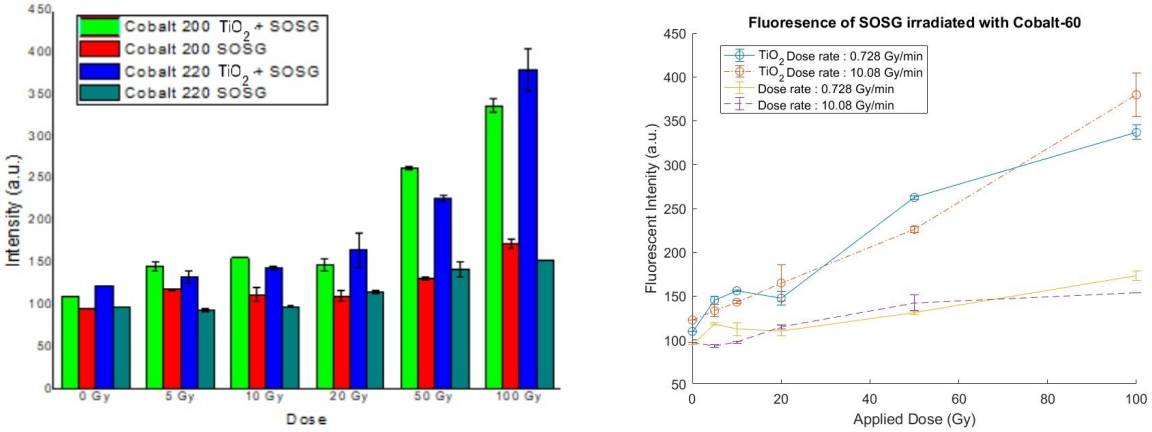


Figure 4.5: A bar plot and linear plot of the fluorescent intensity of a centrifuged SOSG (5 $\mu$M) solution with and without $TiO_2$ (0.5 g/l) after being irradiated with two different $^{60}$Co sources. The $^{60}$Co 200 has a dose rate of 0.728 Gy/min while the $^{60}$Co 220 source has a dose rate of 10.08 Gy/min. Standard deviation applied based on variations between samples.

It is clear that the effect of dose rate is minimal even at higher doses which should enhance possible differences. It is also clear that presence of $TiO_2$ results in a much higher intensity than without $TiO_2$ being present.

No dose rate dependence is visible for both high and low photon energy irradiation regardless of the presence of $TiO_2$. The amount of ROS produced at a given time during radiolysis does not appear to play a role in the chemical enhancement of the SOSG fluorescent signal. The presence of $TiO_2$ however does clearly impact the fluorescent intensity.

### 4.1.3. Photon Energy

Varying photon energies have been applied in effort to gain an understanding whether the production of singlet oxygen is favourable towards an energy range. If $TiO_2$ is used as a dose enhancing agent, it is important to know which photon energies result in the most enhancement. Physical enhancement, pathway A in figure 4.1, is expected to favour lower photon energies for which $TiO_2$ has a relatively large absorption cross section.

Two different experiments were conducted. The first being a comparison between two different X-ray spectra with the same dose rate. The second being a comparison between an X-ray spectrum and the $^{60}$Co source. The experiments were performed with and without the presence of $TiO_2$ NPs.

The two X-ray spectra which are compared have a peak energy of 140 and 230 keV. The 140 keV peak energy was used in combination with a filter which gives an average energy of 83 keV when using a 100 keV peak energy. The average energy therefore lies somewhere between 83 keV and 140 keV. The 230 keV peak energy had a filter in place which gives an average energy of 100 keV when applying 120 kV. The average photon energy therefore lies between 100 keV and 230 keV. The amperage was altered in order to result in a dose rate of 2.5 Gy/h. Samples with and without $TiO_2$ present were irradiated with a dose of 5 Gy. The results of the fluorescent intensity are given in figure 4.6.

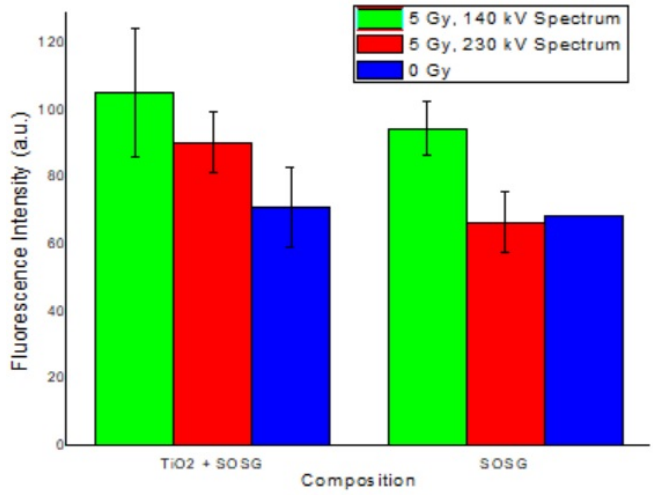


Figure 4.6: Maximal fluorescent emission at 530 nm of SOSG (5$\mu$M) with and without $TiO_2$ (0,25 mg/ml). Both compositions were irradiated with a low energy, 140 kV, and a high enegy, 230 kV, X-ray spectrum. A control set was not irradiated to compare the increase caused by irradiation. Standard deviation applied based on variations between samples.

The results show that a low X-ray spectrum results in an increased fluorescent intensity compared to the high X-ray spectrum. It is important to note that in the case without $TiO_2$ the signal only increases when applying the low energy spectrum.

Because dose rate has shown not to be an important variable, comparisons between the $^{60}$Co source and the X-ray spectra can be made on photon energy alone. The $^{60}$Co 220 source which emits photon at 1.17 and 1.3 MeV had a dose rate around 10.08 Gy/min at the day of the experiment. The X-ray spectrum had a peak energy of 185 keV with a 83 keV filter put in place. The dose rate of the X-ray spectrum is 6.4 Gy/h. The experiment was conducted with and without the presence of $TiO_2$ NPs. The results are given in figure 4.7.

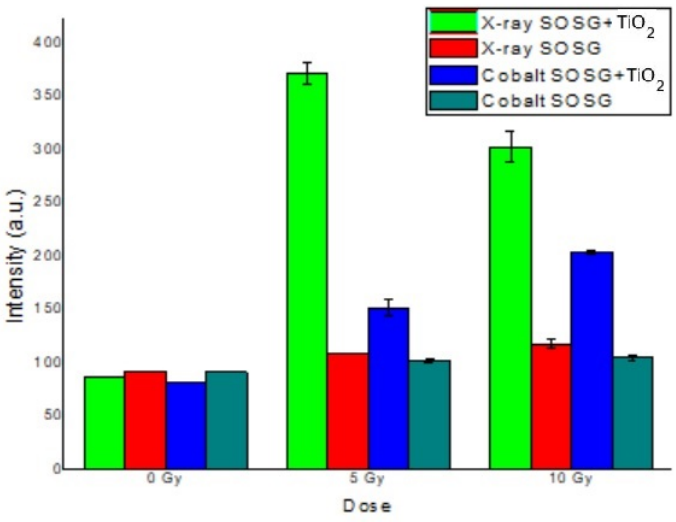


Figure 4.7: Maximal fluorescent emission at 530 nm of SOSG (5$\mu$M) with and without $TiO_2$ (0,25 mg/ml). Both compositions were irradiated with a X-ray spectrum of 185 keV peak energy and 6.4 Gy/h dose and a $^{60}$Co source with a dose rate of 10,08 Gy/min. The samples are grouped based on received dose. A control group was not irradiated, 0 Gy. Standard deviation applied based on variations between samples.

Similar to the comparison between the two X-ray spectra, an increased fluorescent signal is measured for a photon irradiation with lower energies. The increase in fluorescent signal also strongly correlates to the presence of $TiO_2$. The question arises whether the increased fluorescent signal is a result of an increased energy deposition in the solution or a result of some chemical interaction by the $TiO_2$.

The mass attenuation of $TiO_2$ exceeds that of water for energies around the X-ray spectrum. The difference between the materials at photon energies produced by a $^{60}Co$ source are insignificant. The values for these mass attenuations are given in figures 4.8 and 4.9.

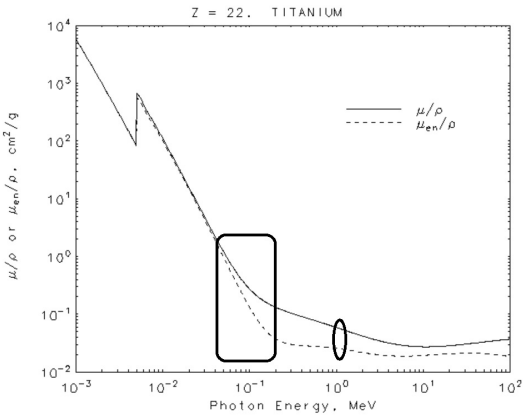


Figure 4.8: Mass attenuation of Titanium as a function of photon energy. The square highlights the energy range of the 185 keV X-ray spectrum and the oval highlights the energy range at 1.17 and 1.33 MeV.

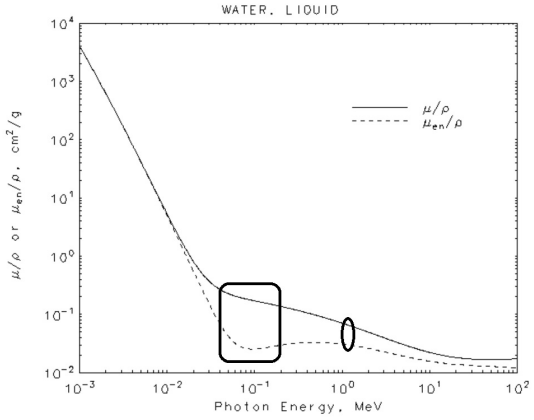


Figure 4.9: Mass attenuation of water as a function of photon energy. The square highlights the energy range of the 185 keV X-ray spectrum and the oval highlights the energy range at 1.17 and 1.33 MeV.

The increased mass attenuation of titanium does not translate to a significant increase in linear attenuation due to the small $TiO_2$ concentration. To arrive at the linear photon attenuation, the mass attenuation has to be multiplied with the density as can been seen in equation 4.2.

$$I = I_0 * \exp(\mu x) \tag{4.1}$$

$$\mu = \sum \mu_i \rho_i \tag{4.2}$$

The $TiO_2$ concentration or density is 0.25 mg/ml which is insignificant compared to water at 1g/ml. This leads to the conclusion that in both cases the vast majority of the photon energy is deposited through interactions with water. From this we must conclude that physical enhancement is not the reason for the increase in fluorescent intensity. Lower photon energies result in a higher signal due to more energy being deposited compared to higher photon energies.

### 4.1.4. Surface Effects

The proposed reaction producing singlet oxygen occurs on the surface of the NP. In an attempt to exclude any chemical reactions, $TiO_2$ NPs with an inert layer were purchased. This inert layer would leave physical enhancement, pathway A in figure 4.1, as the only remaining mechanism. The covered NPs had a different crystalline composition. Instead of being P25 Degussa, 15 % anatase and 85 % rutile, the particles were 80-90 % anatase. NPs with the same composition as the silica covered NPs without the silica layer were also purchased and used as a reference. The goal of the experiments was to block the interactions at the NPs surface to better understand whether the increase in fluorescence is a result of a reaction on the surface or something else.

As a measurement of how well the inert layer blocks the singlet oxygen production of $TiO_2$, an experiment was conducted in room light. An aqueous SOSG solution will not produce an increased fluorescent signal when exposed to room light. The increase must be the result of the interaction of

$TiO_2$, room light and the SOSG. The experiment was conducted with P25, the standard used throughout, silica covered anatase and anatase $TiO_2$ NPs. The results are given in figure 4.10.

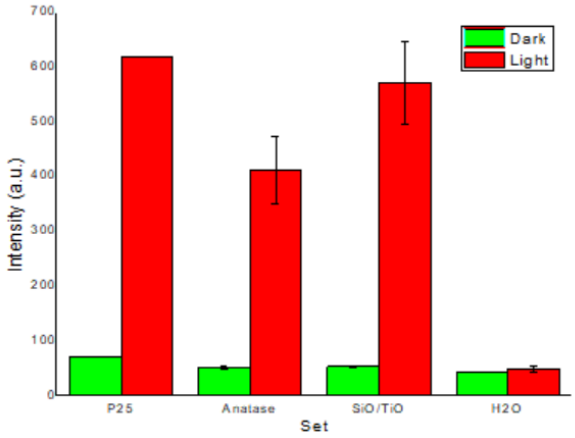


Figure 4.10: Maximal fluorescent emission at 530 nm of SOSG (5$\mu$M) with different crystalline compositions of $TiO_2$ (0,25 mg/ml) and a control set containing SOSG only. The compositions are P25, Anatase and SiO/$TiO_2$ which is anatase $TiO_2$ covered with a silica layer. All compositions were exposed to ambient light. A control group was exposed in order to compare the effect. Standard deviation applied based on variations between samples.

It is clear the silica layer, SiO/TiO, does not inhibit the rise in fluorescence of the SOSG probe. In fact the fluorescent intensity of silica covered $TiO_2$ exceeds that of the uncovered anatase $TiO_2$. This leads to the conclusion that it is not possible to block surface effects using these NPs.

The silica covered and uncovered anatase $TiO_2$ NPs were also irradiated with X-rays with an peak energy of 185 keV. The results as well as the comparison with P25 is visible in figure 4.11.

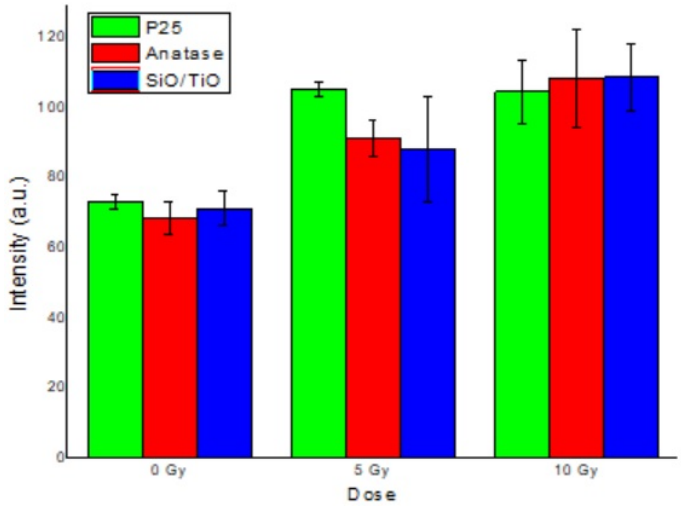


Figure 4.11: Maximal fluorescent emission at 530 nm of SOSG (5$\mu$M) with different crystalline compositions of $TiO_2$ (0,25 mg/ml). The compositions are P25, Anatase and SiO/$TiO_2$ which is anatase $TiO_2$ covered with a silica layer. All compositions were irradiated with a 185 keV peak energy X-ray spectrum. A control group was exposed in order to compare the effect. Standard deviation applied based on variations between samples.

The silica covered $TiO_2$ NPs were unable to block an increase in fluorescent intensity as is clear from figure 4.11. This data agrees with the experiment performed in ambient light. The conclusion therefore is that the silica covered NPs do not block the chemical reaction leading to an increased fluorescence of SOSG upon irradiation with ambient light or ionizing photons.

### 4.1.5. Oxygen Presence

The presence of free oxygen in a sample is expected to be crucial in the production of singlet oxygen. If singlet oxygen is indeed formed as presumed, visible in figure 4.1, superoxide radicals are oxidized to form singlet oxygen. The superoxide radicals have two origins the first being the reduction of free molecular oxygen and the second being the oxidation of hydrogen peroxide on the surface of $TiO_2$. Removal of free oxygen in the sample should lead to a decreased superoxide and therefore a decreased singlet oxygen production.

The presence of free oxygen also has another impact, as hydrated electrons are scavenged by free oxygen to form superoxide radicals [62]. The reaction is given in equation 4.3. The removal of oxygen results in an increased hydrated electron concentration. This increased concentration might result in an increase in fluorescence as hydrated electrons are hypothesised but not proven to react with SOSG [61]. The origin of a possible rise in fluorescence needs to be assigned towards an interaction with caution.

$$O_2 + e^-_{aq} \longrightarrow \cdot O_2^- \tag{4.3}$$

In order to achieve anaerobic condition, the $TiO_2$ and SOSG solutions were bubbled with two different gasses and techniques. The first being argon bubbling and the second nitrogen bubbling. The samples were exposed to ambient light conditions as these should lead to no fluorescent signal. This is due to the lack of hydrogen peroxide present when exposed to ambient light leaving the oxidation of free oxygen as the only path. The exposure to ambient light therefore is an excellent measure of successful oxygen removal.

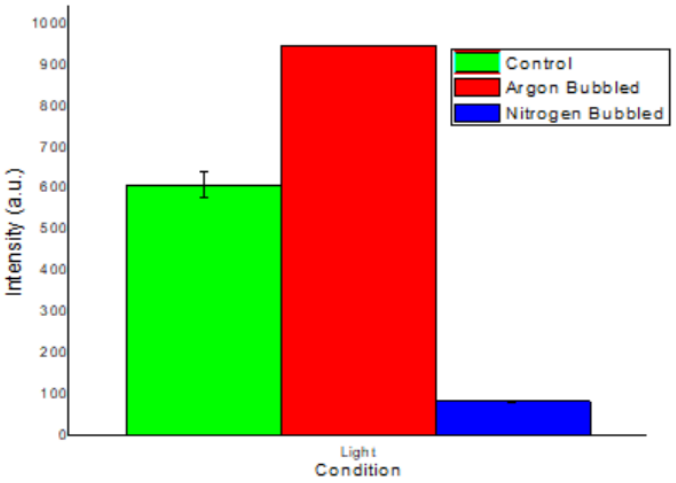


Figure 4.12: Maximal fluorescent emission at 530 nm of SOSG (5$\mu$M) with $TiO_2$ (0,25 mg/ml). All samples were exposed to ambient light for a duration of three hours. Two samples were bubbled using argon or nitrogen in order to remove oxygen and a third set was left untreated as a control. Standard deviation applied based on variations between samples.

The nitrogen bubbled samples resulted in no increased fluorescence upon exposure to ambient light with $TiO_2$ present as is visible in figure 4.12. The argon bubbled samples did result in an increased fluorescent signal comparable to the untreated oxygen rich sample. This leads towards the conclusion that the method and technique used for argon bubbling is not successful in the removal of oxygen while the nitrogen technique is.

The removal of oxygen successfully blocks the increase in fluorescent signal when exposed to ambient light. The same results may be expected when using ionizing radiation. The experiment was conducted using an 185 keV peak energy X-ray spectrum and with the $^{60}$Co 220 source. The results for the X-ray exposure are shown in figure 4.13.

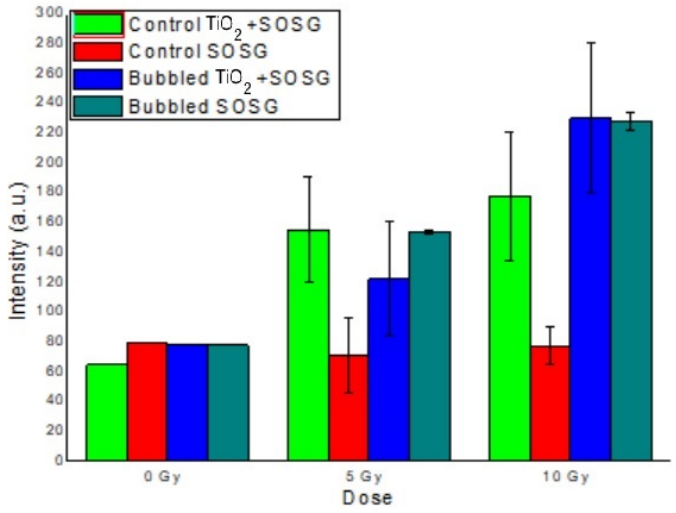


Figure 4.13: Maximal fluorescent emission at 530 nm of SOSG (5$\mu$M) with and without $TiO_2$ (0,25 mg/ml). Half of the samples for both compositions were bubbled with nitrogen to remove free oxygen from the solution. The samples were irradiated with an X-ray spectrum with a peak value at 185 keV and a dose rate of 6,4 Gy/h. The samples are grouped based on received dose. A control group was not irradiated, 0 Gy. Standard deviation applied based on variations between samples.

The nitrogen bubbling did not block the increase in fluorescence as was the case when exposed to ambient light. The removal of oxygen resulted in comparable SOSG signal responses regardless of the presence of $TiO_2$ NPs. This is unlike results previously found where the presence of $TiO_2$ was always significant. This indicates that another process might be dominant, possibly the interaction with hydrated electrons. Another possibility is the production of superoxide radicals by the oxidation of hydrogen peroxide, allowing singlet oxygen to be formed through the original path. However, this reaction path is unlikely since it involves many steps and no effect is visible from the presence of $TiO_2$, which is essential for the oxidation of hydrogen peroxide.

The experiment was also performed using the high dose rate $^{60}$Co 220 source. The dose rate at the time of the experiment was 10.28 Gy/min. The result are given in figure 4.14

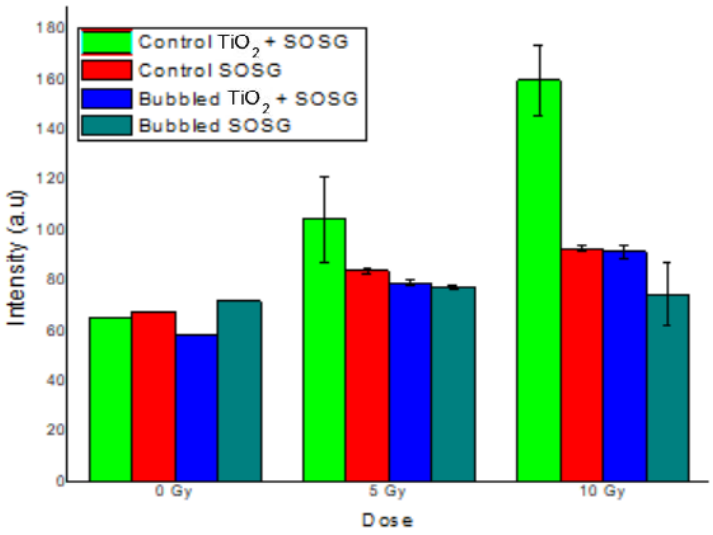


Figure 4.14: Maximal fluorescent emission at 530 nm of SOSG (5$\mu$M) with and without $TiO_2$ (0.25 mg/ml). Half of the samples for both compositions were bubbled with nitrogen to remove free oxygen from the solution. The samples were irradiated with a $^{60}$Co source with a dose rate of 10.28 Gy/min. The samples are grouped based on received dose. A control group was not irradiated, 0 Gy. Standard deviation applied based on variations between samples.

Comparable to the X-ray irradiated case, the presence of $TiO_2$ does not influence the fluorescent intensity in the anaerobic case. However unlike the X-ray irradiated counterpart, the increase in the anaerobic case is insignificant and comparable to the oxygen rich sample without $TiO_2$ present.

This difference is explained on the basis of hydrated electrons. The increase in fluorescent intensity for the X-ray irradiated anaerobic samples could be the result of an interaction of the probe with hydrated electrons. This reaction was expected to be possible but not proven by H. Liu and P. Carter [61]. The lack of response for the $^{60}Co$ irradiated anaerobic samples is explained due to the decreased linear absorption of water at these $\gamma$-ray energies compared to X-ray energies.

The presence of NPs could increase the amount of hydrated electrons significantly due to physical enhancement, as per pathway C in figure 4.1. The interaction of gold NPs and irradiation have shown a large increase in electrons around the NPs due to Auger cascades. These electrons will result in a very high dose and radiolysis, thereby producing hydrated electrons. This effect however is very local and close to the NPs [29]. The presence of $TiO_2$ NPs does not influence the fluorescent intensity in anaerobic conditions implying a possible Auger cascading effect does not impact the SOSG.

The rise in fluorescence in the aerobic case is therefore not likely to be due to hydrated electrons produced by radiolysis or an interaction with the $TiO_2$ NPs. The rise is the result of an interaction facilitated by $TiO_2$ NPs in the presence of oxygen, implying the production of singlet oxygen through the reduction of superoxide radicals.

### 4.1.6. Radical Presence

The production of singlet oxygen is expected to occur with an intermediate step, a superoxide radical. Removal of these radicals should lead to a stop in singlet oxygen production. The following experiments use radical scavengers in order to remove superoxide radicals from the solution. The radical scavengers which are used are HEPES and ascorbic acid, better known as vitamin C.

HEPES is used because it has shown radical scavenging properties in the past. It is important to make sure HEPES itself will not produce a fluorescent signal. This was checked but no fluorescence was measured when using an excitation wavelength of 504 nm. Three solutions containing $TiO_2$ (0.25 mg/ml) and SOSG (5$\mu$M) were prepared. Two of these also had a HEPES concentration of 1 and 10 mM, the third had no HEPES. The samples were exposed to different X-ray doses with a peak energy of 185 keV with a dose rate of 6.4 Gy/h. The results are given in figure 4.15

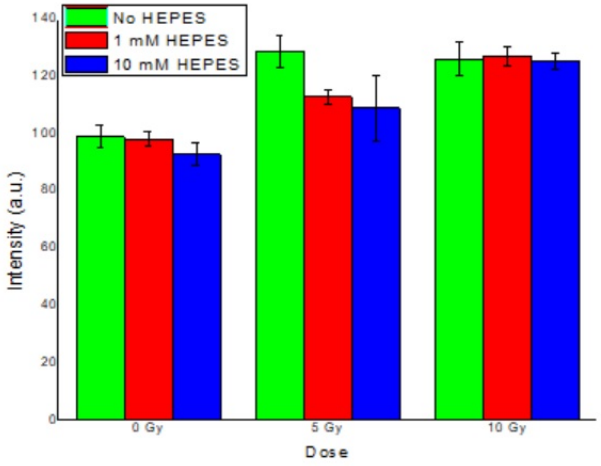


Figure 4.15: Maximal fluorescent emission at 530 nm of a SOSG (5$\mu$M) with $TiO_2$ (0.25 mg/ml), solution. Three sets with different concentrations of HEPES (0, 1 and 10 mM) were irradiated. The samples were irradiated with a X-ray spectrum, peak energy : 185 keV, dose rate : 6.4 Gy/h. The samples are grouped based on received dose 0, 5 and 10 Gy. Standard deviation applied based on variations between samples.

The presence of HEPES, visible in figure 4.15, does not impact the fluorescent intensities significantly. The intensities are similar for all HEPES concentrations used. No conclusion can be drawn about the effectiveness of HEPES as a radical quencher or the necessity of superoxide radicals in the solution.

Ascorbic acid (AA) was also used as a radical quencher. Literature showed that a concentration of 5 mM is needed to successfully quench superoxide radicals [63]. A set of samples containing SOSG (5 $\mu$M) and a set containing SOSG (5 $\mu$M) and $TiO_2$ (0.25 g/l) were prepared in an aqueous solution and a solution containing AA (5 mM). The samples were irradiated with the high dose rate $^{60}$Co source. A dose of 0, 10, 20, 50 and 100 Gy were applied at a dose rate of 9.8 Gy/min. The results are given in figure 4.16

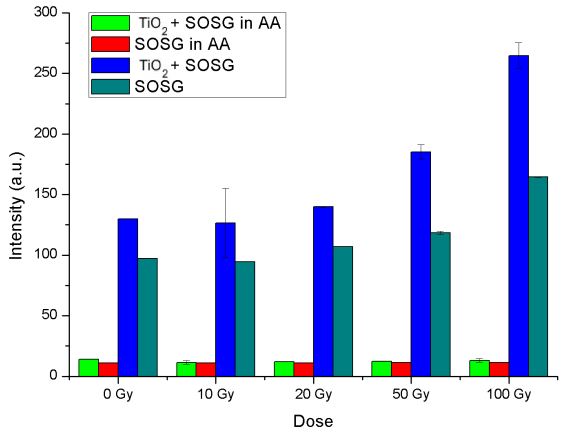


Figure 4.16: Maximal fluorescent emission at 530 nm of a SOSG (5$\mu$M) with $TiO_2$ (0.25 mg/ml), solution in asorbic acid (AA, 5 mM) or aqueous solution. The samples were irradiated with a $^{60}$Co source, dose rate : 9.8 Gy/min. The samples are grouped based on received dose 0, 10, 20, 50 and 100 Gy. Standard deviation applied based on variations between samples.

As can be seen in figure 4.16 the AA completely killed the fluorescent signal of SOSG. The pH was measured as this might be the origin of the signal loss. The pH in the ascorbic acid samples was around 3.6 $\pm$ 0.1 regardless of the dose applied.

## 4.2. Mythelene Blue

Mythelene blue is used as an indicator for the ability of $TiO_2$ NPs to oxidize their surroundings. The oxidation of MB results in a measurable UV-Vis shift. The shift in absorbance of MB was measured from 770 nm down to 200 nm in steps of 1 nm using a UV-6300PC Double Beam spectrophotometer. The solutions of the MB were checked and possibly diluted before measuring to ensure the 0 Gy sample set had an absorbance below 1 as this is the most accurate region [60].

The oxidation of superoxides is expected to be crucial in the production of singlet oxygen. The X-ray source, compared to the $^{60}Co$ source, led to the highest SOSG fluorescence, which should indicate the presence of singlet oxygen. Because the production of singlet oxygen is expected to be linked to the oxidative abilities of $TiO_2$, these circumstances are expected to result in the most oxidation of its surroundings. Therefore all radiation, unless specified otherwise, was applied using the X-ray source with a peak photon energy of 185 keV and a dose rate of 6.4 Gy/h, in attempt to achieve the most oxidation. Different variables were applied and discussed in the following sections.

### 4.2.1. Ambient Light

The first experiments were performed under ambient light conditions to verify that $TiO_2$ had the desired effect on MB. 1 ml samples were prepared containing MB (0,01 g/l) and $TiO_2$ (0.25 g/l). The samples were exposed to ambient light for different amounts of time after which they were centrifuged to remove the $TiO_2$. A control set was kept in the dark for the same amount of time in order to circumvent possible aggregation uncertainties. The UV-Vis absorbance of the samples were measured resulting in the following for the ambient light conditions.

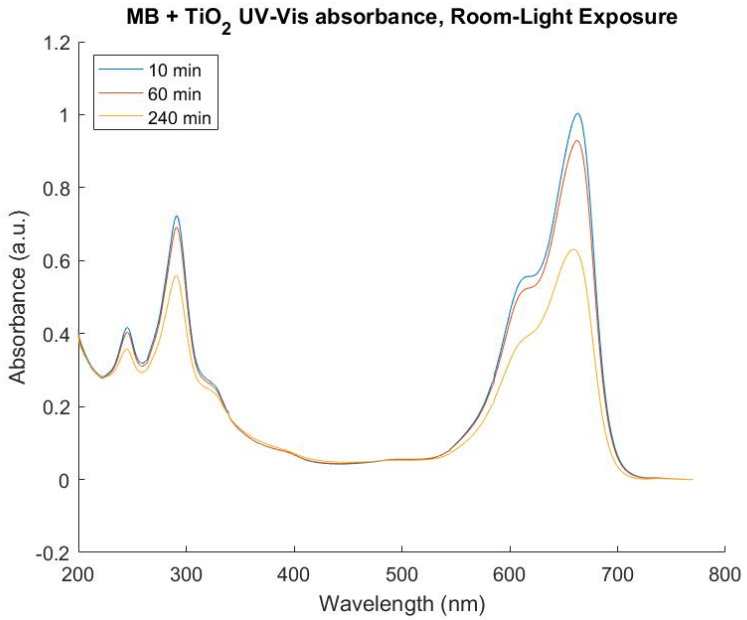


Figure 4.17: UV-Vis absorbance of a Myhelene Blue (0.01 g/l) and $TiO_2$ (0.25 g/l) solution, from 200 nm up to 770 nm. Samples were exposed to ambient light for a duration of 10, 60 and 240 minutes.

As is clear in figure 4.17 a decrease in absorbance is measured at the expected peaks. However the time needed for a significant amount of degradation to occur is relatively long, 2 hours. For the dark conditions the following UV-Vis spectrum was measured.

As can be seen in figure 4.18 a slight increase after 10 minutes is measured. This results further complicates comparisons between samples exposed less than 1 hour. When comparing the results after 10 minutes the absorbance of the light exposed samples increased at 655 nm which is not in agreement with the literature which show a small decrease [64]. After an exposure of 60 minutes a drop in MB absorbance is measurable but this drop is in the order of a few percent.

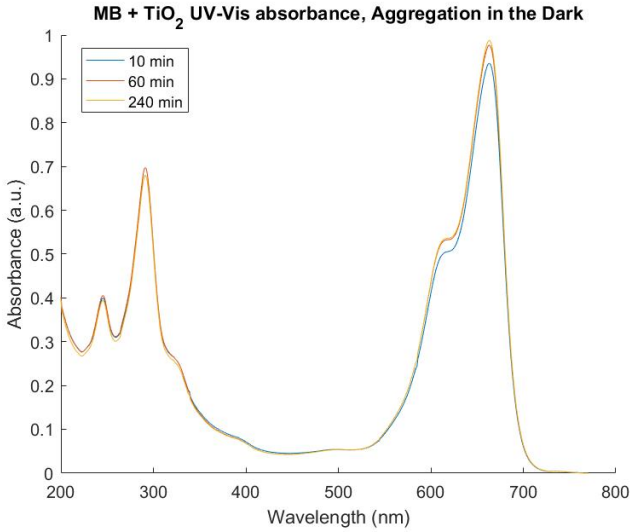


Figure 4.18: UV-Vis absorbance of a Myhelene Blue (0.01 g/l) and $TiO_2$ (0.25 g/l) solution, from 200 nm up to 770 nm. Control set to the ambient light exposed samples. The samples were kept in the dark for a duration of 10, 60 and 240 minutes in order to mimic possible aggregation in the ambient light exposed samples.

### 4.2.2. Radical Quencher

The first question, when using irradiation, is whether the measured degradation is the result of formed radicals or the electron holes produced in $TiO_2$. This is important as the presence of electrons holes as a result of being exposed to radiation enforces the proposed singlet oxygen production path. The radical quencher HEPES was added to half the samples containing MB and $TiO_2$ and irradiated. The difference in degradation should be due to the lack of radicals, leaving the electron hole pairs as the only cause. The samples were exposed to 0, 5 and 10 Gy. The results for the set without the radical quencher are given in figure 4.19 and the set with HEPES are given in figure 4.20.

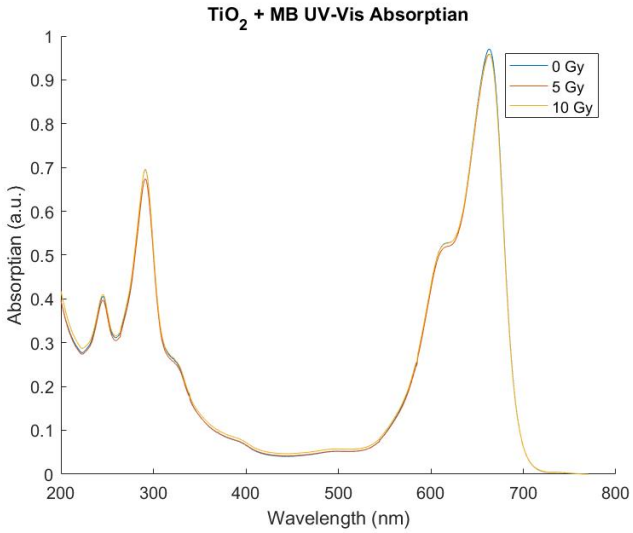


Figure 4.19: UV-Vis absorbance of a Myhelene Blue (0.01 g/l) and $TiO_2$ (0.25 g/l) solution, from 200 nm up to 770 nm. Samples were irradiated with an X-ray spectrum, 185 keV peak energy and a dose rate of 6.8 Gy/h, up to 5 and 10 Gy.

It is clear from figure 4.19 that irradiating MB in the presence of $TiO_2$ with X-rays resulted in almost no difference in absorbance spectra. This can be the result of a very limited sensitivity of the MB at the doses used or that $TiO_2$ in combination with radiation is not capable of degrading MB.

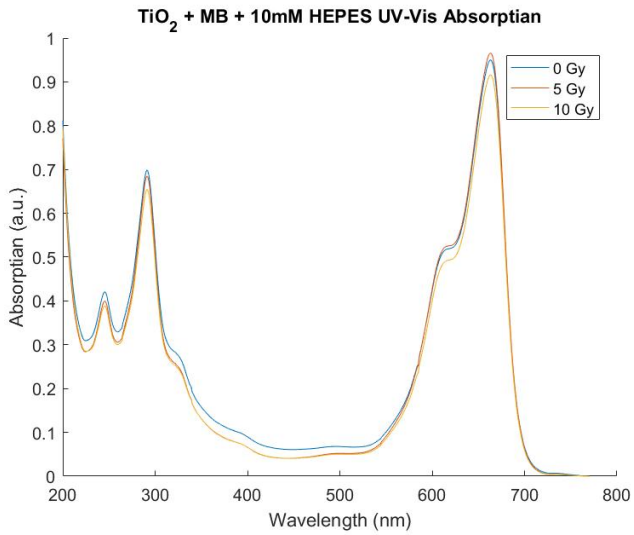


Figure 4.20: UV-Vis absorbance of a Myhelene Blue (0.01 g/l), $TiO_2$ (0.25 g/l) and radical quencher HEPES (10 mM) solution, from 200 nm up to 770 nm. Samples were irradiated with an X-ray spectrum, 185 keV peak energy and a dose rate of 6.8 Gy/h, up to 5 and 10 Gy.

When looking at the case with HEPES present in figure 4.20 bigger differences are visible. The 5 Gy irradiated set increased in absorbance at the 633 nm peak while the 10 Gy decreased compared to the non irradiated set. Looking at the rest of the spectrum a decrease in absorbance at 300 nm is visible with increasing dose. The general elevation of the spectrum however is decreased in the irradiated cases which does correspond to the degradation of MB, possibly leading to shifts at other regions of the spectrum.

No conclusions on the effect of the presence of radicals when degrading MB with a combination $TiO_2$ and irradiation can be drawn.

### 4.2.3. Anaerobic Conditions

Another method to remove ROS from the solution in order to verify the origin of the degradation of MB is to remove the oxygen. Removing the oxygen from the solution inhibits the production of ROS which rely on the presence of free oxygen. The solutions containing MB and $TiO_2$ were bubbled with nitrogen to remove the oxygen.

The UV-Vis absorbance after bubbling was measured in order to verify no strange effects occurred. The process of removing oxygen resulted in a decrease in MB concentration as is visible in figure 4.21. This is the result of MB loss through the gas outlet in the set-up. Over time some blue liquid concentrated at the gas outlet indicating a clear loss of concentration in the solution.

Although some concentration may be lost during the nitrogen bubbling process, no further obstacles emerged. The bubbled MB and $TiO_2$ solution were irradiated with the X-ray source up to 10 Gy. The results are given below in figure 4.22 and can be compared to the non bubbled results given in figure 4.19.

The initial intensities are lower than the non bubbled cases showcasing the loss of MB during the bubbling process. The influence of the radiation is however very unexpected. In contrast to an expected decline in absorbance as a result of the oxidation of MB, an increase is measured. This could imply that in stead of oxidizing, some LMB (oxidized MB) is reduced back into MB. However this could also be the result of residual $TiO_2$ left in the sample.

No conclusion on the influence of removing oxygen can be made.

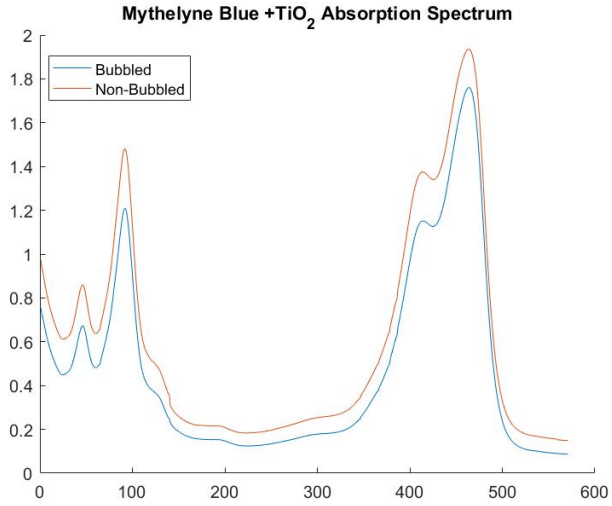


Figure 4.21: V-Vis absorbance of a nitrogen bubbled and non-bubbled Myhelene Blue (0.01 g/l) and $TiO_2$ (0.25 g/l) solution, from 200 nm up to 770 nm.

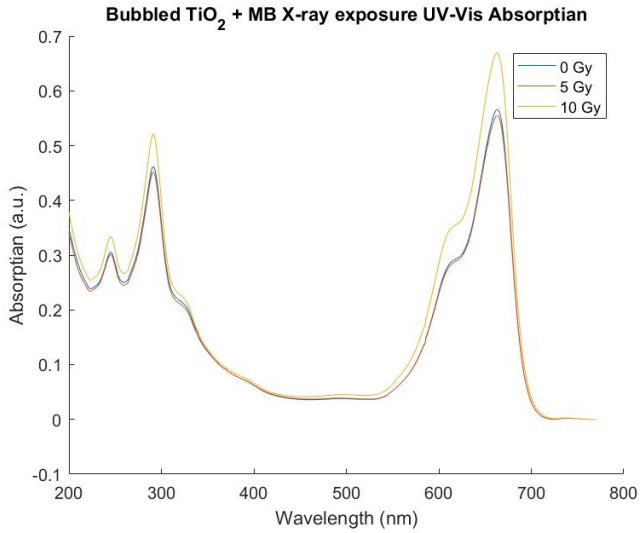


Figure 4.22: UV-Vis absorbance of a nitrogen bubbled Myhelene Blue (0.01 g/l) and $TiO_2$ (0.25 g/l) solution, from 200 nm up to 770 nm. Samples were irradiated with an X-ray spectrum, 185 keV peak energy and a dose rate of 6.8 Gy/h, up to 5 and 10 Gy.

### 4.2.4. Surface Effects

The possibility for the spontaneous decomposition of MB as the result of trapped holes on the titanium surface has been shown to be possible. This is the result of the decomposition of hydrogen peroxide into hydroxyl radicals. The trapped holes could substitute the role of the electron hole pairs in the production of singlet oxygen. Hydrogen peroxide is formed during radiolysis. Therefore it is of interest to investigate whether such trapped holes can be measured when adding hydrogen peroxide in concentrations comparable to the amount produced during radiolysis.

The amount of produced hydrogen peroxide is approximately 2.5 and 5 $\mu$M when exposed to 5 and 10 Gy with the X-ray source. The samples were kept in the dark as to see whether spontaneous decomposition occurred. The results are given in figure 4.23

As is clear from figure 4.23, no decrease in absorbance is measured when hydrogen peroxide is added. The amounts of $H_2O_2$ produced is not enough to start the spontaneous decomposition of MB. This however does not exclude a small shift in the energy band gap.

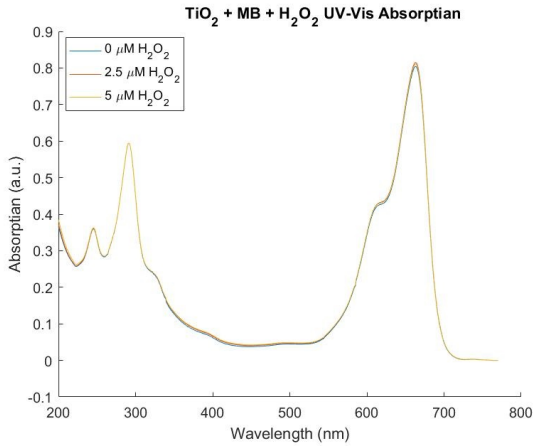


Figure 4.23: UV-Vis absorbance of Myhelene Blue (0.01 g/l) and $TiO_2$ (0.25 g/l) solution, from 200 nm up to 770 nm. Different amounts of hydrogen peroxide, $H_2O_2$, are added to the solutions, 2.5 and 5 $\mu$M. The samples were kept in dark conditions as the degradation should be the result of spontaneous degradation.

### 4.2.5. Cobalt 60

In order to achieve higher doses the samples must be irradiated with the $^{60}$Co source due to its dose rate. The $^{60}$Co 220 source was used to reach a maximum dose of 100 Gy. The $^{60}$Co 220 source had a dose rate of 10 Gy/min during the experiment. The pure MB samples are given in figure 4.24 and the MB samples with $TiO_2$ are given in figure 4.25.

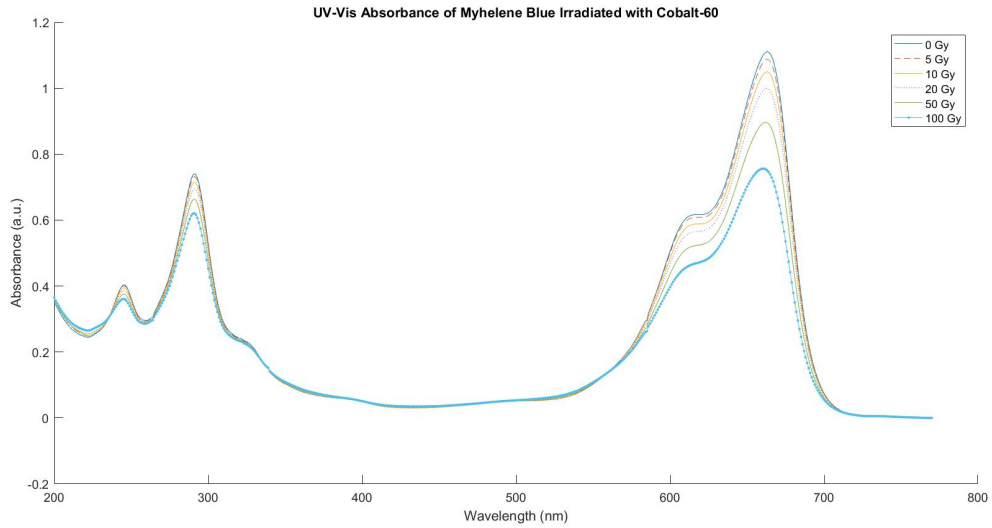


Figure 4.24: UV-Vis absorbance of a Myhelene Blue (0.01 g/l) solution, from 200 nm up to 770 nm. Samples were irradiated with a $^{60}$Co source, 10 Gy/min, up to 5, 10, 20 ,50 and a 100 Gy.

The degradation of MB clearly increases with higher doses regardless of the presence of $TiO_2$. The amount of degradation at doses below 10 Gy are not very distinctive and comparable to the X-ray irradiated samples.

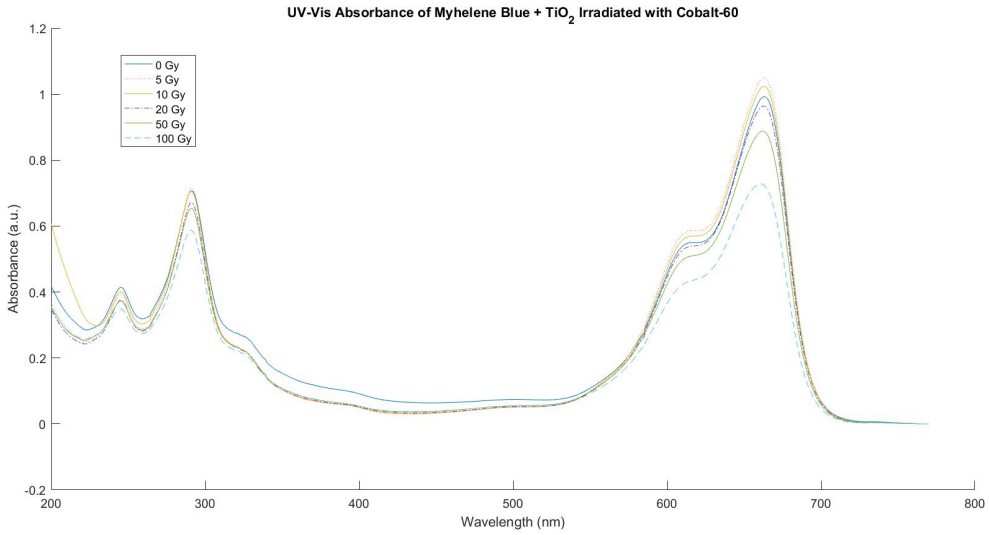


Figure 4.25: UV-Vis absorbance of a Myhelene Blue (0.01 g/l) and $TiO_2$ (0.25 g/l) solution, from 200 nm up to 770 nm. Samples were irradiated with a $^{60}$Co source, 10 Gy/min, up to 5, 10, 20 ,50 and a 100 Gy.

It however difficult to directly compare the cases with $TiO_2$ present and without. Figure 4.26 gives the degradation of MB as a percentage of the original absorbance at 663 nm which is the peak value. The degradation is a function of dose.

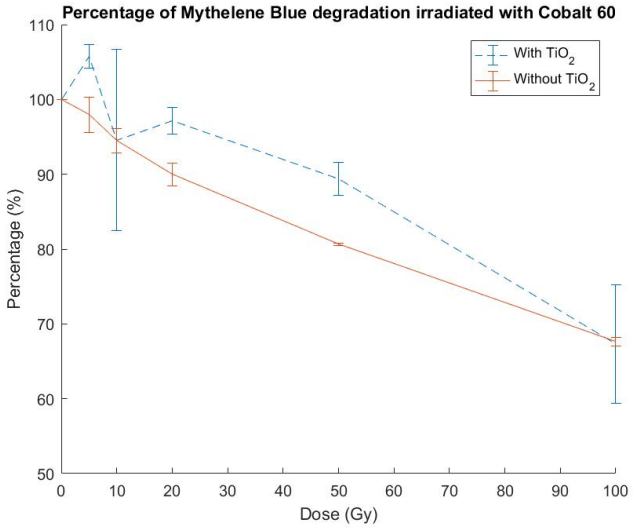


Figure 4.26: The percentile degradation of MB (0.01 g/l) as a function of dose. The absorbance is compared at 663 nm. The original absorbance at 0 Gy is set as 100 %, after which a percentile degradation is shown. The blue dotted line is in the presence of $TiO_2$ (0.25 g/l) and the red solid line is pure MB. Standard deviation applied based on variations between samples.

As is clear in figure 4.26 the degradation does not depend on the presence of $TiO_2$ and increases with received dose. The degradation of MB is most probably the result of radicals produced during radiolysis.

# 5

# Conclusion & Recommendations

## 5.1. Conclusion

The fluorescent probe SOSG has consistently shown a significant rise in fluorescent intensity when irradiated in the presence of oxygen and $TiO_2$ NPs. The rise in fluorescence appears to be linked to the presence of singlet oxygen but this could not be concluded.

The necessity for aerobic conditions when $TiO_2$ is exposed to ambient light to result in a fluorescent SOSG signal leads to the conclusion that $TiO_2$ produces ROS. The ROS which are directly affected by the presence of oxygen are superoxide radicals and singlet oxygen. The manufacturer of SOSG claims low reactivity for the superoxide radicals, leaving singlet oxygen as the only possibility.

Replicating this experiment with ionizing photon irradiation shows different results depending on the photon energy used. This is explained as a result of the amount of energy deposited into the system due to different linear absorption coefficients for different photon energies. An additional product formed during radiolysis compared to photocatalysis are hydrated electrons, $e^-_{aq}$, which appear to react with SOSG resulting in a high fluorescent signal. The rise in fluorescence of SOSG due to hydrated electrons does not depend on the presence of $TiO_2$ but on the presence of free oxygen, as these normally absorb the hydrated electrons creating superoxide radicals. Because the presence of $TiO_2$ NPs does not influence the results in anaerobic conditions, no production of hydrated electrons by the interactions of ionizing radiation with the NPs are expected for both anaerobic and aerobic conditions. Leaving the increase in fluorescence in aerobic conditions with $TiO_2$ NPs present, to singlet oxygen or an unknown interaction.

The mechanisms behind the production of singlet oxygen could not be uncovered. Experiments on possible surface effects, using particles covered with an inert layer, and free radical dependence, using radical scavengers such as HEPES or ascorbic acid, did not result in additional knowledge on the mechanisms. It is however clear that the fluorescent intensity of the probe does not depend on dose rate and does favor lower photon energies.

Mythelene Blue degradation experiments were performed to verify whether irradiation is capable of forming electron hole pair in $TiO_2$. The degradation of MB is not in the same order of sensitivity as SOSG, meaning much higher doses are needed in order to achieve significant results. The presence of $TiO_2$ in a 0.25 (g/l) concentration does not enhance the degradation of MB, leading to the conclusion that no significant amount degradation is caused by the photocatalytic activity of this $TiO_2$ concentration.

## 5.2. Recommendations

After my experiments it remains unclear whether the rise in fluorescent signal is due to singlet oxygen. Singlet oxygen appears to be the logical origin for the rise in fluorescent signal but this could not be verified. A mass spectrum measurement is capable of verifying this. The absorption of singlet oxygen results in an additional mass of 32 u. This difference is measurable and could only be attributed towards singlet oxygen absorption. This method was attempted in this thesis, but due to unknown errors a very strange mass spectrum emerged leaving the data useless. Very high mass were measured, which were not present in the sample.

As to uncovering the origin of the possible singlet oxygen production, there are other ways of determining whether electron hole formations occur under irradiation which might be more sensitive such as electrical current measurements [43]. The surface effects should also be successfully blocked in order to gain a better understanding whether the reaction takes place here. This is possible by covering the $TiO_2$ NPs yourself with a silica layer or searching another supplier.

# A

# Appendix

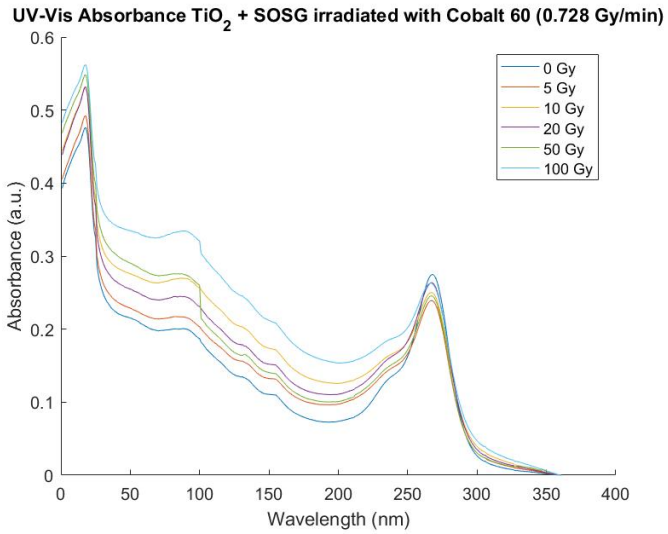


Figure A.1: UV-Vis absorbance of SOSG irradiated with a Cobalt 60 source in the presence of $TiO_2$ NPs.

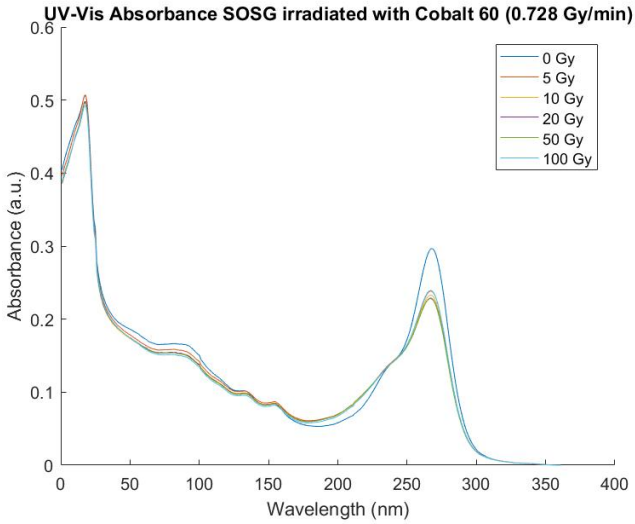


Figure A.2: UV-Vis absorbance of SOSG irradiated with a Cobalt 60 source in the presence of $TiO_2$ NPs.

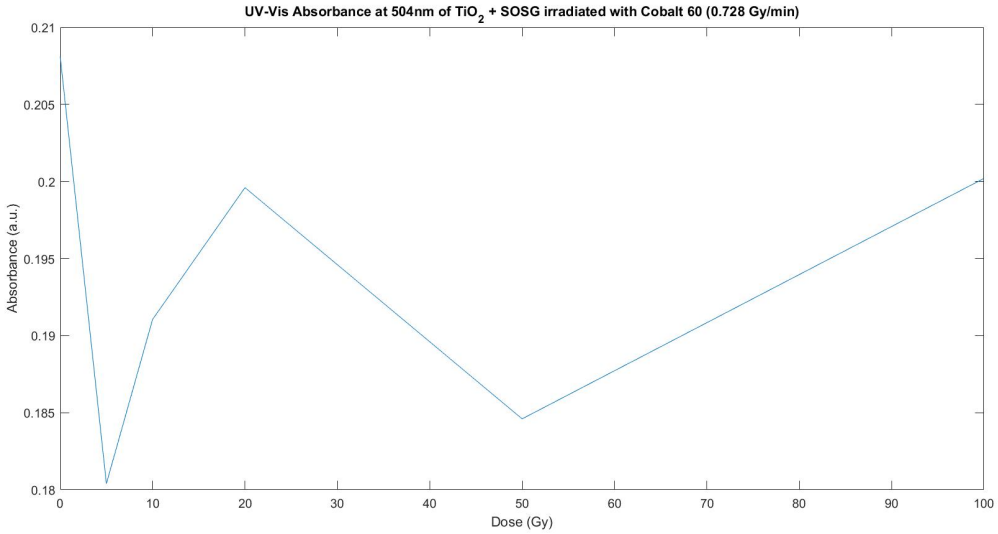


Figure A.3: UV-Vis absorbance of SOSG (5 $\mu$M) at 504 nm as a function of dose received from a Cobalt 60 source. The SOSG solution was in contact with $TiO_2$ NPs during irradiation which were removed before the UV-Vis measurement.

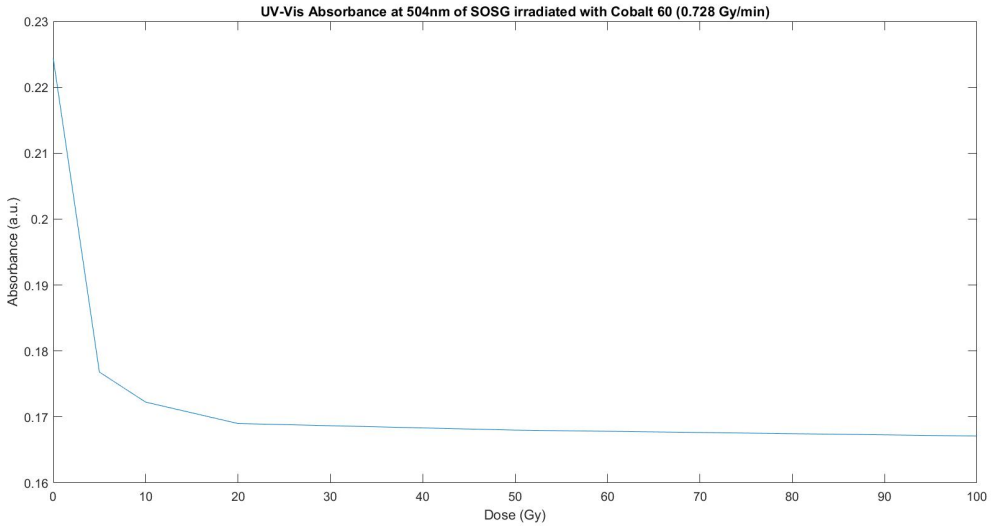


Figure A.4: UV-Vis absorbance of SOSG (5 $\mu$M) at 504 nm as a function of dose received from a Cobalt 60 source.

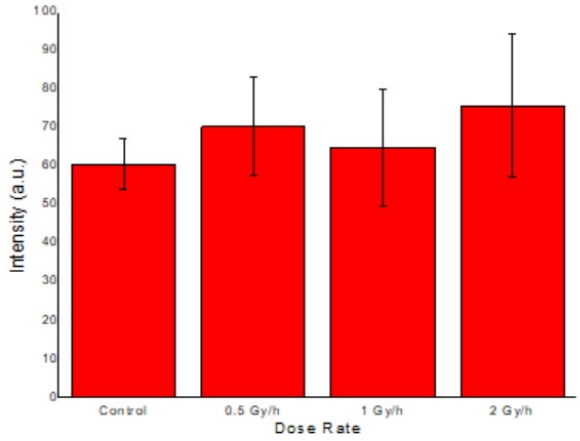


Figure A.5: Fluorescent intensity of a centrifuged SOSG (5 $\mu$M molar) irradiated with a 140 keV peak energy X-ray spectrum. Samples received 1 Gy with a variable dose rate, from left to right 2, 1 and 0.5 Gy/h, and a control sample which received no radiation. Standard deviation applied based on variations between samples.

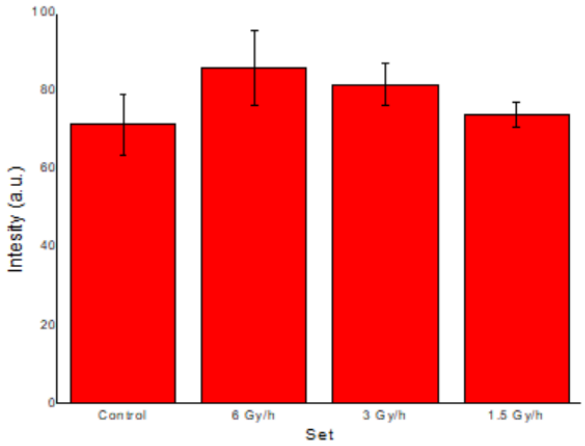


Figure A.6: Fluorescent intensity of a centrifuged SOSG (5 $\mu$M molar) irradiated with a 185 keV peak energy X-ray spectrum. Samples received 3 Gy with a variable dose rate, from left to right 6, 3 and 1.5 Gy/h, and a control sample which received no radiation. Standard deviation applied based on variations between samples.

# Bibliography


[1] R. Baskar, K. A. Lee, R. Yeo, and K.-W. Yeoh, "Cancer and radiation therapy: current advances and future directions," *International journal of medical sciences*, vol. 9, no. 3, p. 193, 2012.

[2] L. C. Brown, R. W. Mutter, and M. Y. Halyard, "Benefits, risks, and safety of external beam radiation therapy for breast cancer," *International journal of women's health*, vol. 7, p. 449, 2015.

[3] S. M. Huber, L. Butz, B. Stegen, L. Klumpp, D. Klumpp, and F. Eckert, "Role of ion channels in ionizing radiation-induced cell death," *Biochimica et Biophysica Acta (BBA) - Biomembranes*, vol. 1848, no. 10, Part B, pp. 2657 – 2664, 2015. Membrane Channels and Transporters in Cancers.

[4] "Stereotactic radiotherapy of malignancies in the abdomen: methodological aspects,"

[5] M. C. Ferris and M. M. Voelker, "Fractionation in radiation treatment planning," *Mathematical programming*, vol. 101, no. 2, pp. 387–413, 2004.

[6] T. Guo, *X-ray nanochemistry: concepts and development*. Springer, 2018.

[7] G. Ou, Z. Li, D. Li, L. Cheng, Z. Liu, and H. Wu, "Photothermal therapy by using titanium oxide nanoparticles," *Nano Research*, vol. 9, no. 5, pp. 1236–1243, 2016.

[8] D. Kalyane, N. Raval, R. Maheshwari, V. Tambe, K. Kalia, and R. K. Tekade, "Employment of enhanced permeability and retention effect (epr): Nanoparticle-based precision tools for targeting of therapeutic and diagnostic agent in cancer," *Materials Science and Engineering: C*, vol. 98, pp. 1252 – 1276, 2019.

[9] A. Ben Mihoub, L. Larue, A. Moussaron, Z. Youssef, L. Colombeau, F. Baros, C. Frochot, R. Vanderesse, and S. Acherar, "Use of cyclodextrins in anticancer photodynamic therapy treatment," *Molecules*, vol. 23, no. 8, 2018.

[10] U. S. Srinivas, B. W. Tan, B. A. Vellayappan, and A. D. Jeyasekharan, "Ros and the dna damage response in cancer," *Redox Biology*, vol. 25, p. 101084, 2019. Redox Regulation of Cell State and Fate.

[11] C. Sicard-Roselli, E. Brun, M. Gilles, G. Baldacchino, C. Kelsey, H. McQuaid, C. Polin, N. Wardlow, and F. Currell, "A new mechanism for hydroxyl radical production in irradiated nanoparticle solutions," *small*, vol. 10, no. 16, pp. 3338–3346, 2014.

[12] A. Wold, "Photocatalytic properties of titanium dioxide (tio2)," *Chemistry of Materials*, vol. 5, no. 3, pp. 280–283, 1993.

[13] M. C. DeRosa and R. J. Crutchley, "Photosensitized singlet oxygen and its applications," *Coordination Chemistry Reviews*, vol. 233-234, pp. 351–371, 2002.

[14] E. Q. Youkhana, B. Feltis, A. Blencowe, and M. Geso, "Titanium dioxide nanoparticles as radiosensitisers: an in vitro and phantom-based study," *International Journal of Medical Sciences*, vol. 14, no. 6, p. 602, 2017.

[15] M. v. d. B. N. Ebink, E. Theunissen, "Ros formation with tio2 irradiated by low energy x-rays and high-energy gamma-rays," *Paculty of Applied Sciences, Delft University of Technology, The Netherlands*, 2020.

[16] A. Zamanian and C. Hardiman, "Electromagnetic radiation and human health: A review of sources and effects," *High Frequency Electronics*, vol. 4, no. 3, pp. 16–26, 2005.

[17] J. v. d. E. &. M. Schouwenburg, *Practical Radiation Protection*. Syntax Media - Utrecht, third ed., 2013.

[18] M. A. Heald and J. B. Marion, *Classical electromagnetic radiation*. Courier Corporation, 2012.

[19] "Nuclear power, collaberation of engineers in effort to distribute information. taken at 18-2-2021,"

[20] J. BIRKS, "Chapter 2 - absorption of the incident radiation," in *The Theory and Practice of Scintillation Counting* (J. BIRKS, ed.), International Series of Monographs in Electronics and Instrumentation, pp. 15 – 38, Pergamon, 1964.

[21] G. Choppin, J.-O. Liljenzin, and J. Rydberg, *Radiochemistry and nuclear chemistry*. Butterworth-Heinemann, 2002.

[22] I. Draganic, *The radiation chemistry of water*, vol. 26. Elsevier, 2012.

[23] D. Féron, *Nuclear corrosion science and engineering*. Elsevier, 2012.

[24] N. P. Contributors, "Radiation."

[25] C. Lousada, I. Soroka, Y. Yagodzinskyy, N. Tarakina, O. Todoshchenko, H. Hänninen, P. Korzhavyi, and M. Jonsson, "Gamma radiation induces hydrogen absorption by copper in water open," *Scientific Reports*, vol. 6, pp. 1 – 8, 04 2016.

[26] N. J. Green and S. M. Pimblott, "Radiation track structure simulation in a molecular medium," *Research on Chemical Intermediates*, vol. 27, no. 4-5, pp. 529–538, 2001.

[27] C. T. R. Wilson, "Investigation on x-rays and $\beta$-rays by the cloud method. part ii.—$\beta$-rays," *Proceedings of the Royal Society of London. Series A, Containing Papers of a Mathematical and Physical Character*, vol. 104, no. 725, pp. 192–212, 1923.

[28] S. M. Pimblott and A. Mozumder, "Structure of electron tracks in water. 2. distribution of primary ionizations and excitations in water radiolysis," *The Journal of Physical Chemistry*, vol. 95, no. 19, pp. 7291–7300, 1991.

[29] K. T. Butterworth, S. J. McMahon, F. J. Currell, and K. M. Prise, "Physical basis and biological mechanisms of gold nanoparticle radiosensitization," *Nanoscale*, vol. 4, no. 16, pp. 4830–4838, 2012.

[30] V. Kanike, J. Meesungnoen, and J.-P. Jay-Gerin, "Acid spike effect in spurs/tracks of the low/high linear energy transfer radiolysis of water: potential implications for radiobiology," *RSC Adv.*, vol. 5, pp. 43361–43370, 2015.

[31] D. E. Watt, *Quantities For Generalized Dosimetry of Ionizing Radiations in Liquid Water*. CRC Press, 2003.

[32] J. Schneider, M. Matsuoka, M. Takeuchi, J. Zhang, Y. Horiuchi, M. Anpo, and D. W. Bahnemann, "Understanding tio2 photocatalysis: mechanisms and materials," *Chemical reviews*, vol. 114, no. 19, pp. 9919–9986, 2014.

[33] M. Bodzek and M. Rajca, "Photocatalysis in the treatment and disinfection of water. part i. theoretical backgrounds," *Ecological Chemistry and Engineering. S = Chemia i Inżynieria Ekologiczna. S*, vol. 19, pp. 489–512, 12 2012.

[34] Y. Nosaka and A. Y. Nosaka, "Generation and detection of reactive oxygen species in photocatalysis," *Chemical reviews*, vol. 117, no. 17, pp. 11302–11336, 2017.

[35] S. Kohtani, A. Kawashima, and H. Miyabe, "Reactivity of trapped and accumulated electrons in titanium dioxide photocatalysis," *Catalysts*, vol. 7, no. 10, p. 303, 2017.

[36] M. C. DeRosa and R. J. Crutchley, "Photosensitized singlet oxygen and its applications," *Coordination Chemistry Reviews*, vol. 233, pp. 351–371, 2002.

[37] T. Devasagayam and J. P. Kamat, “Biological significance of singlet oxygen,” 2002.

[38] Y. You, “Chemical tools for the generation and detection of singlet oxygen,” *Org. Biomol. Chem.*, vol. 16, pp. 4044–4060, 2018.

[39] V. A. Sharpatyi and I. Kraljić, “Detection of singlet oxygen in radiolysis of aerated aqueous solutions,” *Photochemistry and Photobiology*, vol. 28, no. 4-5, pp. 587–590, 1978.

[40] E. B. Podgorsak, “External photon beams: Physical aspects,” *Radiation Oncology Physics: A handbook for teachers and students’. Vienna: IAEA*, p. 169, 2005.

[41] C. M. Lousada Patrício, *Reactions of aqueous radiolysis products with oxide surfaces: An experimental and DFT study*. PhD thesis, KTH Royal Institute of Technology, 2013.

[42] X. Li, C. Chen, and J. Zhao, “Mechanism of photodecomposition of h2o2 on tio2 surfaces under visible light irradiation,” *Langmuir*, vol. 17, no. 13, pp. 4118–4122, 2001.

[43] Y. Rao and W. Chu, “Reaction mechanism of linuron degradation in tio2 suspension under visible light irradiation with the assistance of h2o2,” *Environmental science & technology*, vol. 43, no. 16, pp. 6183–6189, 2009.

[44] M.-C. Lee, F. Yoshino, H. Shoji, S. Takahashi, K. Todoki, S. Shimada, and K. Kuse-Barouch, “Characterization by electron spin resonance spectroscopy of reactive oxygen species generated by titanium dioxide and hydrogen peroxide,” *Journal of dental research*, vol. 84, no. 2, pp. 178–182, 2005.

[45] L. D. Sánchez, S. F. M. Taxt-Lamolle, E. O. Hole, A. Krivokapić, E. Sagstuen, and H. J. Haugen, “Tio2 suspension exposed to h2o2 in ambient light or darkness: Degradation of methylene blue and epr evidence for radical oxygen species,” *Applied Catalysis B: Environmental*, vol. 142, pp. 662–667, 2013.

[46] K. C. Ko, S. T. Bromley, J. Y. Lee, and F. Illas, “Size-dependent level alignment between rutile and anatase tio2 nanoparticles: implications for photocatalysis,” *The Journal of Physical Chemistry Letters*, vol. 8, no. 22, pp. 5593–5598, 2017.

[47] A. Y. Ahmed, T. A. Kandiel, T. Oekermann, and D. Bahnemann, “Photocatalytic activities of different well-defined single crystal tio2 surfaces: anatase versus rutile,” *The Journal of Physical Chemistry Letters*, vol. 2, no. 19, pp. 2461–2465, 2011.

[48] Y. Kakuma, A. Y. Nosaka, and Y. Nosaka, “Difference in tio 2 photocatalytic mechanism between rutile and anatase studied by the detection of active oxygen and surface species in water,” *Physical Chemistry Chemical Physics*, vol. 17, no. 28, pp. 18691–18698, 2015.

[49] S. Le Caër, “Water radiolysis: influence of oxide surfaces on h2 production under ionizing radiation,” *Water*, vol. 3, no. 1, pp. 235–253, 2011.

[50] R. Essehli, F. Crumière, G. Blain, J. Vandenborre, F. Pottier, B. Grambow, M. Fattahi, and M. Mostafavi, “H2 production by $\gamma$ and he ions water radiolysis, effect of presence tio2 nanoparticles,” *International Journal of Hydrogen Energy*, vol. 36, no. 22, pp. 14342–14348, 2011.

[51] H. N. McQuaid, M. F. Muir, L. E. Taggart, S. J. McMahon, J. A. Coulter, W. B. Hyland, S. Jain, K. T. Butterworth, G. Schettino, K. M. Prise, *et al.*, “Imaging and radiation effects of gold nanoparticles in tumour cells,” *Scientific reports*, vol. 6, no. 1, pp. 1–10, 2016.

[52] S. J. McMahon, W. B. Hyland, M. F. Muir, J. A. Coulter, S. Jain, K. T. Butterworth, G. Schettino, G. R. Dickson, A. R. Hounsell, J. M. O’Sullivan, *et al.*, “Nanodosimetric effects of gold nanoparticles in megavoltage radiation therapy,” *Radiotherapy and Oncology*, vol. 100, no. 3, pp. 412–416, 2011.

[53] S. Kim, M. Fujitsuka, and T. Majima, “Photochemistry of singlet oxygen sensor green,” *The journal of physical chemistry B*, vol. 117, no. 45, pp. 13985–13992, 2013.

[54] A. Gollmer, J. Arnbjerg, F. H. Blaikie, B. W. Pedersen, T. Breitenbach, K. Daasbjerg, M. Glasius, and P. R. Ogilby, "Singlet oxygen sensor green®: photochemical behavior in solution and in a mammalian cell," *Photochemistry and photobiology*, vol. 87, no. 3, pp. 671–679, 2011.

[55] C. Hou, B. Hu, and J. Zhu, "Photocatalytic degradation of methylene blue over tio2 pretreated with varying concentrations of naoh," *Catalysts*, vol. 8, no. 12, p. 575, 2018.

[56] R. Zuo, G. Du, W. Zhang, L. Liu, Y. Liu, L. Mei, and Z. Li, "Photocatalytic degradation of methylene blue using tio2 impregnated diatomite," *Advances in Materials Science and Engineering*, vol. 2014, 2014.

[57] "Titanium oxide nanoparticles (anatase/rutile, 20 nm)."

[58] "Titanium oxide, silica coated (anatase/rutile, 20 nm)."

[59] "Singlet oxygen sensor green - special packaging."

[60] T. Mayerhöfer, S. Pahlow, and J. Popp, "The bouguer-beer-lambert law: Shining light on the obscure," *ChemPhysChem*, vol. 21, 07 2020.

[61] L. Huanhuan, C. P. JH, A. C. Laan, E. Rienk, and A. G. Denkova, "Singlet oxygen sensor green is not a suitable probe for 1 o 2 in the presence of ionizing radiation," *Scientific Reports (Nature Publisher Group)*, vol. 9, no. 1, 2019.

[62] "Principles of radiation interaction, taken at 19-8-2020,"

[63] A. E. Wagner, P. Huebbe, T. Konishi, M. M. Rahman, M. Nakahara, S. Matsugo, and G. Rimbach, "Free radical scavenging and antioxidant activity of ascorbigen versus ascorbic acid: studies in vitro and in cultured human keratinocytes," *Journal of agricultural and food chemistry*, vol. 56, no. 24, pp. 11694–11699, 2008.

[64] T. Tran, T. Quach, Q. Tran, T. Nguyen, N. Chien, D. Manh, D. Tran, N. Nguyễn, V. Tuyen, and D. Le, "Synthesis of vanadium-modified rutile tio 2 nanoparticle by reactive grinding method and its photocatalytic activity under solar light at room temperature," *Advances in Natural Sciences: Nanoscience and Nanotechnology*, vol. 4, p. 035010, 09 2013.